Key

ENTERED

Earthquake scenario and probabilistic ground-shaking hazard maps for the Albuquerque–Belen–Santa Fe, New Mexico, corridor

Ivan Wong,[1] *Susan Olig,*[1] *Mark Dober,*[1] *Walter Silva,*[2] *Douglas Wright,*[1] *Patricia Thomas,*[1] *Nick Gregor,*[2] *Allan Sanford*[3], *Kuo-wan Lin*[4], and *David Love*[5],
[1]Seismic Hazards Group, URS Corporation, 1333 Broadway, Suite 800, Oakland, CA 94612;
[2]Pacific Engineering & Analysis, 311 Pomona Avenue, El Cerrito, CA 94530;
[3]New Mexico Institute of Mining and Technology, Socorro, NM 87801;
[4]California Geological Survey, California Department of Conservation, 801 K Street, MS 13-35, Sacramento, CA 95814;
[5]New Mexico Bureau of Geology and Mineral Resources, Socorro, NM 87801

Abstract

New Mexico's population is concentrated along the corridor that extends from Belen in the south to Española in the north and includes Albuquerque and Santa Fe. The Rio Grande rift, which encompasses the corridor, is a major tectonically, volcanically, and seismically active continental rift in the western U.S. Although only one large earthquake (moment magnitude [M] ≥ 6) has possibly occurred in the New Mexico portion of the rift since 1849, paleoseismic data indicate that prehistoric surface-faulting earthquakes of M 6.5 and greater have occurred on average every 400 yrs on many faults throughout the Rio Grande rift.

We have developed a series of nine scenario and probabilistic hazard maps that portray the ground shaking that could occur in the Albuquerque–Belen–Santa Fe corridor from future earthquakes in New Mexico. These maps, at a scale of 1:500,000, display color-contoured ground-motion values in terms of the parameters of peak horizontal acceleration and horizontal spectral accelerations at 0.2 and 1.0 second (sec) periods. The maps depict surficial ground shaking and incorporate the site-response effects at locations underlain by unconsolidated sediments. The scenario maps are for a M 7.0 earthquake rupturing the Sandia–Rincon faults, which are adjacent to and dip west beneath Albuquerque. The probabilistic maps are for the two annual exceedance probabilities of building code relevance, 10% and 2% exceedance probabilities in 50 yrs (corresponding to return periods of 500 and 2,500 yrs, respectively).

We included 57 Quaternary faults, all located within the Rio Grande rift, in the probabilistic seismic hazard analysis. These faults were characterized in terms of their geometry, rupture behavior (including possible segmentation), maximum expected earthquake magnitude, recurrence model, probability of activity, and slip rate. Preferred maximum magnitude values for these faults ranged from M 6.1 to 7.4 and preferred slip rates from 0.01 to approximately 0.12 mm/yr. Regional source zones and Gaussian smoothing of the historical seismicity were also included in the probabilistic hazard analysis to account for the hazard from background earthquakes (M ≤ 6.5).

A numerical ground-motion modeling approach and empirical attenuation relationships appropriate for extensional tectonic regimes were used to compute the scenario earthquake and probabilistic ground motions on rock. Amplification factors were then used to modify the rock motions and hence to incorporate site response into the hazard maps. These factors were based on three generalized geologic site-response categories (hard rock, soft rock, and firm/stiff soil) and were adopted from similar California-based categories because insufficient subsurface geologic and geotechnical data are available for the map area.

The resulting hazard maps indicate that from both scenario and probabilistic perspectives, the ground-shaking hazard in the Albuquerque–Belen–Santa Fe corridor from future earthquakes could be severe, damaging, and potentially disastrous. In the event of a M 7.0 earthquake occurring on the Sandia–Rincon faults, ground shaking as characterized by peak ground acceleration could reach 0.7 g in much of the eastern half of the Albuquerque metropolitan area. (1 g = 980 cm/sec^2, the rate of gravitational acceleration.) These high ground motions will be attributable to the city's location directly over the Sandia–Rincon faults and the amplifying effect of the unconsolidated sediments within the Albuquerque Basin. These levels of ground shaking will probably result in severe damage to traditional adobe construction and even to modern buildings. Long-period ground motions (> 1.0 sec), which are significant to long and tall structures (e.g., tall buildings, long bridges, and highway overpasses), will also be high (> 1.0 g). Injuries and loss of life will be likely.

For the 500- and 2,500-yr return period maps, the highest peak accelerations are predicted to be at the damaging levels of 0.3 g and 0.6 g, respectively. All maps show dramatically the frequency-dependent amplification of unconsolidated sediments in the basins along the Rio Grande valley (e.g., Albuquerque Basin). The pattern of amplification and deamplification is clearly a function of the distribution of unconsolidated sediments.

These maps are not intended to be a substitute for site-specific studies for engineering design nor to replace standard maps commonly referenced in building codes. Rather, we hope that these maps will be used as a guide by government agencies; the engineering, urban planning, emergency preparedness, and response communities; and the general public as part of an overall program to reduce earthquake risk and losses in New Mexico.

Limitations

Authors' note: There are significant uncertainties associated with earthquake ground-motion prediction in New Mexico due to limited region-specific information and data on the characteristics of seismic sources and ground-motion attenuation. Additional uncertainty stems from the characterization of the subsurface geology beneath the map area and the estimation of the associated site-response effects on ground motions. Thus the maps should not be used directly for site-specific design or in place of site-specific hazard evaluations.

Introduction

One-half of New Mexico's population of 1.8 million people live along the 175-km-long (110-mi-long) Rio Grande valley corridor that extends from Belen in the south to Española in the north. This corridor includes the major cities of Albuquerque and Santa Fe and parts of Santa Fe, Sandoval, Bernalillo, Los Alamos, and Valencia Counties. The corridor is situated within the Rio Grande rift, a tectonically, volcanically, and seismically active continental rift in the western U.S. (Chapin 1979; Sanford et al. 1991; Fig. 1). Although only one earthquake larger than moment magnitude (M) 6 may have occurred in New Mexico in historical times (since 1849), paleoseismic data indicate that prehistoric surface-faulting earthquakes of M 6.25 and greater have occurred on many faults throughout the rift (Machette et al. 1998; Machette 1998).

Based on the most up-to-date information on seismic sources, crustal attenuation, and near-surface geology, we have estimated strong ground shaking for the Albuquerque–Belen–Santa Fe corridor. Recent information on Quaternary faulting and revised historical earthquake catalogs for New Mexico for the period 1869 through 1998 (Sanford et al. 2002; Fig. 1) were used in the hazard analyses. Small-magnitude background seismicity not associated with known faults is relatively abundant within this part of the Rio Grande rift, and thus moderate-sized background earthquakes (M 5.0–6.5) are included in the hazard evaluations.

Using both deterministic and probabilistic seismic hazard analyses, a total of nine hazard microzonation maps have been produced. These include: earthquake sce-

37148

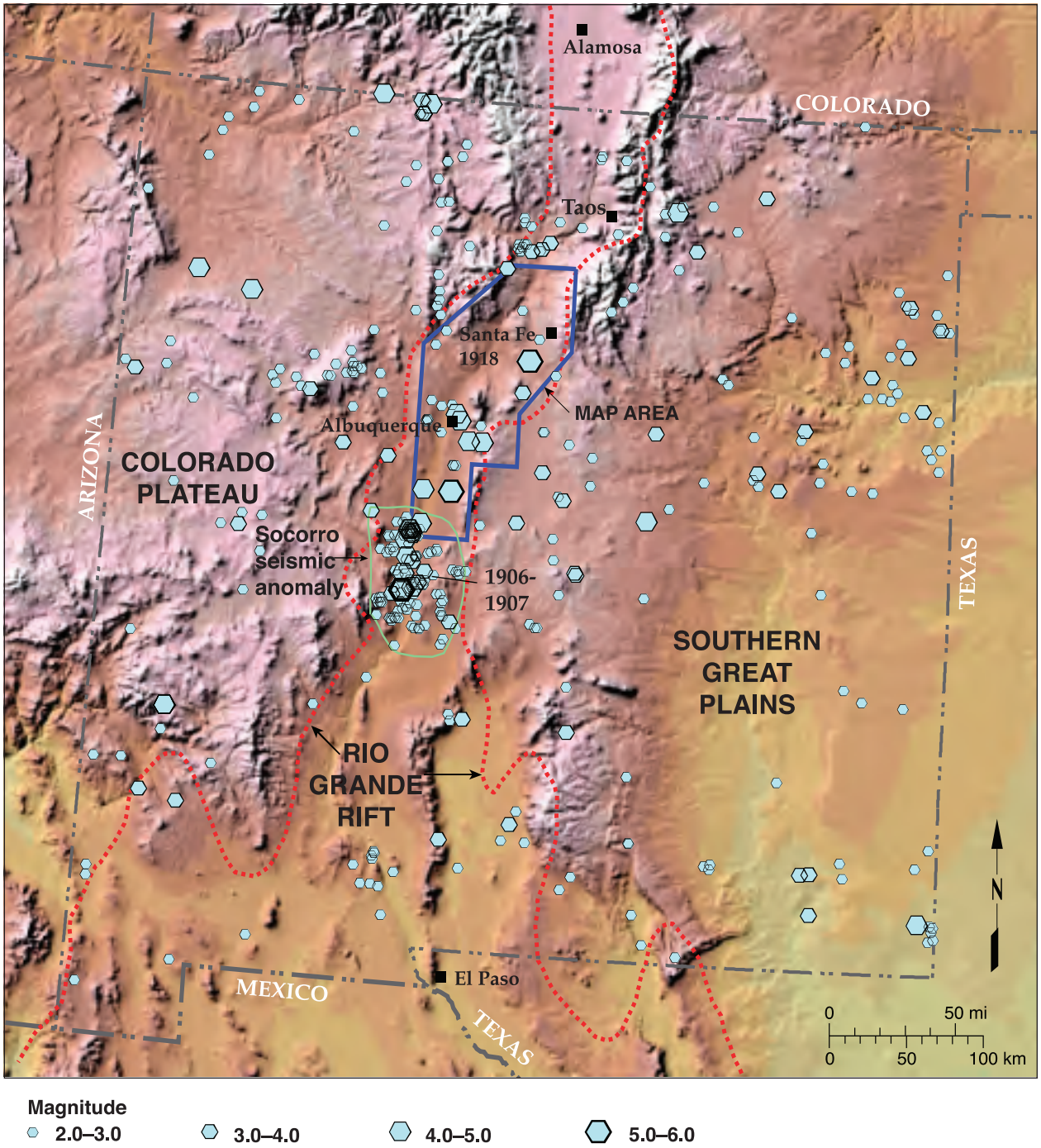

FIGURE 1—Seismotectonic provinces and historical seismicity, 1869 to 1998, in New Mexico. Only independent earthquakes (foreshocks, aftershocks, and smaller swarm events have been removed) used in the probabilistic hazard analysis are shown. The outline of the Rio Grande rift is from Machette (1998).

nario maps for a **M** 7.0 earthquake along the Sandia–Rincon faults just east of Albuquerque and probabilistic maps for the two exceedance probabilities of building code relevance, 10% and 2% probability of exceedance in 50 yrs (mean return periods of 500 and 2,500 yrs, respectively). Although numerous active faults (Personius et al. 1999; Personius and Mahan 2000, 2003) could generate strong earthquake ground shaking in the Albuquerque metropolitan area, the Sandia–Rincon faults earthquake scenario was selected because it may represent the event with the most serious consequences because of its proximity to New Mexico's highest concentration of population.

The ground parameter chosen to illustrate the severity of ground shaking is spectral acceleration expressed in terms of g's. The GIS-based maps display peak horizontal acceleration (zero period) and horizontal spectral accelerations at periods of 0.2 and 1.0 sec (5 Hz and 1 Hz frequencies, respectively) at the ground surface.

The maps are intended to illustrate the intensity and variability of ground shaking within the map area for the scenario earthquake as well as for two exceedance probabilities. It is our hope that these maps will be used by all those interested in earthquake hazard mitigation in the Albuquerque–Belen–Santa Fe corridor. The maps are intended for a number of uses such as increasing general public awareness of earthquake hazards, urban planning, selecting facility sites, assisting in mitigation planning for lifelines, and aiding emergency preparedness, response, and loss estimation. Although we believe the maps represent the state-of-the-art in ground-motion modeling for the region,

the maps are not intended to be used directly in engineering design. Various codes such as the Uniform Building Code and International Building Code define minimum design ground-motion levels for buildings and other structures, and commonly reference other maps (e.g., Frankel et al. 2002) to determine these design levels. Our maps do not replace these maps or site-specific design studies, but they can be used to compare with code-based design and to evaluate the need for increasing design levels if indicated.

Although the intended users of these maps will vary in their technical knowledge, the following article by its very nature is a technical description of the approach used in the map development and some important aspects of the resulting maps. For additional information, please contact the senior author (ivan_wong@urscorp.com).

Seismotectonic setting and historical seismicity

The Rio Grande rift in north-central New Mexico and south-central Colorado is a broad physiographic and structural depression bordered by the southern Rocky Mountains to the north, the Colorado Plateau transition zone to the west, and the Great Plains to the east (Fig. 1). The rift in north-central New Mexico is composed of a series of north-trending, elongate topographic and structural basins that are collapsed parts of a broad area of Laramide structural uplift (Baltz 1978). The structural basins are arranged in a right-stepping, en echelon pattern, and are characterized by high heat flow, abundant late Quaternary faults, Quaternary volcanism, and thick accumulations of basin sediment fill (Morgan et al. 1986). From north to south, the basins in north-central New Mexico are the San Luis, Española, Santo Domingo, and Albuquerque Basins. In general, these basins are broad half-grabens as much as 80 km wide (50 mi wide) that are generally tilted either to the east or west and typically have a deep, narrow inner graben.

The Rio Grande rift exhibits geologic and geophysical characteristics that are similar to other continental rifts throughout the world, such as the Kenya rift of the East African rift system and the Baikal rift of the Mongolian Plateau (Keller et al. 1991). The Rio Grande rift, like the Kenya rift, is an example of continental rifting associated with lithospheric thinning and upwelling of the asthenosphere (Davis 1991; Keller et al. 1991). Both rifts are associated with regions of broad uplift and arching, with elevations of rift flanks locally as high as 4 km (2.5 mi). Gravity, seismic refraction, and other geophysical studies show that the lithospheric mantle is anomalously thin or absent beneath the axes of the Rio Grande and Kenya rifts. The replacement of mantle lithosphere beneath the rifts with warm, buoyant asthenospheric mantle probably accounts for the regional elevated topography, high heat flow, low gravity, and late Cenozoic magmatism (Keller et al. 1991).

Historical seismicity

Sanford et al. (1991) have summarized the results of several detailed studies of seismicity in the Rio Grande rift of New Mexico (see Sanford et al. 2002 for an updated description of the historical seismicity). In general, seismicity is diffuse and only locally associated with discrete structural or tectonic features. Detailed studies of the Albuquerque and Socorro areas show that seismicity is limited to the upper 12–13 km (7.5–8 mi) of the crust (Sanford et al. 1991), consistent with observations from other rift systems that seismicity typically is concentrated in the upper crust (Doser and Yarwood 1991). Earthquake focal mechanisms from the Albuquerque and Socorro areas indicate both strike-slip and normal faulting. These data also suggest that the direction of extensional tectonic stress (minimum principal stress) may vary within the rift. Based on focal mechanisms, the orientation of the minimum principal stress is interpreted to be approximately east-west within the rift (Sanford et al. 1991). Sanford et al. (1991) noted that local areas of high seismicity in the Albuquerque area (Fig. 1) may be correlated with magmatic activity rather than tectonism. Notably, Sanford et al. (1991) concluded that modern patterns of seismicity in the Rio Grande rift may not necessarily be representative of long-term activity.

The largest historical event to have occurred within the Rio Grande rift was a **M** 7.4 earthquake in 1887 that ruptured 101 km (63 mi) of the Pitaycachi fault in Sonora, Mexico, just south of the southwestern corner of New Mexico (Machette 1998; Suter and Contreras 2002). The event was felt as far away as Santa Fe to the north; Toluca near Mexico City to the south; Yuma, Arizona, on the west; and 96 km (60 mi) east of El Paso, Texas (DuBois et al. 1982). The total felt area has been estimated at 1.5–2.0 million km^2 (0.6–0.8 million mi^2). The earthquake caused 51 deaths in small communities close to the epicenter from collapsed adobe structures. Many landslides and ground cracks were reported.

In historical times, only six earthquakes of estimated Richter local magnitude (M_L) 5.0 (or Modified Mercalli intensity [MM] VI; see Table 1) or greater have occurred within the Rio Grande rift in New Mexico. The largest historical earthquake was probably the November 15, 1906, earthquake near Socorro (Fig. 1). A wide range of magnitudes has been suggested for this event (M_L 4.9–6.5) due to the large uncertainties of noninstrumental observations (Sanford et al., 1979). The event was felt throughout central New Mexico over an area of approximately 245,000 km^2 (94,600 mi^2; Reid 1911; Sanford et al. 1991). Its maximum intensity was estimated at MM VIII, and it caused additional damage to structures already weakened in previous events on July 12 and 16.

The region around Socorro is known to be the source of intermittent swarms of seismicity possibly due to inflation of a midcrustal magma body (Sanford et al. 1991). The November 15 event was part of a sequence in 1906–1907 that began on July 2, 1906, with two jolting earthquakes in the morning that were felt within an 80 km (50 mi) radius of Socorro (Reid 1911). Earthquakes were then felt almost daily from July 2, 1906, to July 21, 1907, the most severe occurring on July 12, July 16, and November 15, 1906. The July 12 earthquake lasted 15–20 sec, causing adobe walls to crack, some chimneys to fall, and a rockslide to cause some damage to a nearby railroad (MM VII–VIII). Many aftershocks followed, including the July 16 earthquake, which damaged additional chimneys and houses, caused a brick gable to partially fall down, and the southeast corner of a brick post office to be thrown out (Reid 1911).

The 1918 earthquake near the town of Cerrillos is the largest historical earthquake to have occurred within the northern part of the Rio Grande rift (Fig. 1). It was strongly felt in Cerrillos where chimneys fell, plaster cracked, windows broke, people were thrown off their feet, and a large ground crack appeared at the edge of town (Olsen et al. 1979). Olsen et al. (1979) assigned a maximum intensity of MM VII and a magnitude of M_L 5.25 to this earthquake.

Quaternary faulting

In marked contrast to the historical earthquake record, geologic studies of the paleoseismic record in the Rio Grande rift indicate large prehistoric surface-faulting earthquakes (**M** > 6.25) have occurred throughout the rift (Machette 1998). Quaternary (younger than 1.6 m.y.) movement on faults is widespread in the rift and has long been recognized as evidence for large prehistoric earthquakes (e.g., Nakata et al. 1982; Machette 1987). A recent compilation of Quaternary faults in New Mexico includes well over 100 faults in the rift (Machette et al. 1998), with at least 20 of these showing evidence for movement in Holocene time (past 10,000 yrs; Machette 1998).

Many of these faults are major range-bounding normal faults (Machette and Hawley 1996) that show characteristics typical of faults in the Basin and Range province—that is, faults that separate uplifted ranges from down-dropped basins, forming the mountain and intervening valley topography that generally parallels the north-south trending structural fabric of the rift. However, some significant complexities are also superimposed

TABLE 1—Relationship of peak horizontal ground acceleration (PGA) to Modified Mercalli (MM) intensity (adapted from Wald et al. 1999).

MM intensity	Perceived shaking	Damage	PGA(g)
I	Not felt except by a very few under especially favorable circumstances.	None	<<0.01
II	Felt only by a few persons at rest especially on upper floors of buildings.	None	<0.01
III	Felt quite noticeably indoors; especially on upper floors of buildings, but many people do not recognize it as an earthquake.	None	<0.01
IV	During the day felt indoors by many, outdoors by few. At night some awakened.	None	0.01–0.04
V	Felt by nearly everyone, many awakened.	Very light—Some dishes and windows broken; cracked plaster in a few places; unstable objects overturned.	0.04–0.09
VI	Felt by all, many frightened.	Light—Some heavy furniture moved; a few instances of fallen plaster and damaged chimneys.	0.09–0.18
VII	Very strong	Moderate—Damage negligible in buildings of good design and construction; slight to moderate in well-built ordinary structures; considerable in poorly built or badly designed structures; some chimneys broken.	0.18–0.34
VIII	Severe—Persons driving cars disturbed.	Moderate to heavy—Damage slight in specially designed structures; considerable in ordinary substantial buildings with partial collapse; great in poorly built structures. Chimneys toppled.	0.34–0.65
IX	Violent	Heavy—Damage considerable in specially designed structures; well-designed frame structures thrown out of plumb; great in substantial buildings, with partial collapse. Buildings shifted off foundations.	0.65–1.24
X	Extreme	Very heavy—Some well-built wooden structures destroyed; most masonry and frame structures destroyed with foundations.	>1.24
XI	Extreme	Extreme—Few, if any, (masonry) structures remain standing.	>1.24
XII	Extreme	Extreme—Damage total.	>1.24

on this first-order approximation of Quaternary fault patterns. Some of these complexities include: (1) intrabasin faults that may be secondary (e.g., Bernalillo fault) or antithetic (e.g., Rendija Canyon fault) to other structures; (2) intrabasin faults associated with volcanism (e.g., Cat Mesa fault); (3) dominantly strike slip faults that separate right-stepping basins (e.g., Embudo fault) or transect ranges (e.g., Tijeras–Cañoncito fault zone); and (4) intrabasin faults that form complex distributed zones with horsts and grabens (e.g., faults on the Llano de Albuquerque).

Despite these sometimes significant complexities, some generalizations can be made about Quaternary faults in the Rio Grande rift: (1) they have dominantly normal slip, (2) moderate to low slip rates (typically less than 1 mm/yr [0.04 in/yr]), (3) relatively long recurrence intervals between surface-faulting events (typically tens of thousands to hundreds of thousands of years), (4) they generally strike north-south, and (5) typically are poorly understood but often show extreme variations in rates of activity through time (Machette et al. 1998). Although individual faults generally have moderate to low rates of activity, their cumulative effect and the apparent variability in rates of activity through time make it particularly important to include Quaternary faults in seismic hazard evaluations of the rift.

Machette (1998) suggested a Holocene composite recurrence interval for the Rio Grande rift of about 450 yrs based on 22 Holocene surface-rupturing earthquakes. He also cautioned that this number of events is a minimum (and thus the recurrence interval is a maximum), as most of the faults have not been studied in any detail. Indeed his total count did not include recently discovered Holocene events on the Rincon (Connell 1995) and Pajarito faults (McCalpin 1998) thus increasing the count to 24 events and decreasing the composite recurrence interval to about 400 yrs. Large variations in rates of activity through time resulting from temporal clustering of events are recognized for many faults in the rift, and slip rates for some faults vary by more than an order of magnitude through time (McCalpin 1995).

Including these variations has a measurable impact on the probabilistic hazard analysis by increasing uncertainties and generally raising hazard levels. Unfortunately, because relatively few faults have been studied in enough detail to determine adequate paleoseismic histories, we know even less about what causes temporal clustering and the degree to which it actually occurs on individual faults and throughout the rift.

Methodology and input to hazard calculations

There were five principal tasks in the development of the hazard maps: (1) seismic source characterization; (2) definition and characterization of geologic site-response categories and assignment of amplification factors; (3) seismic attenuation characterization; (4) scenario and probabilistic ground-motion calculations; and (5) map development using GIS.

Seismic source characterization

The first step in any assessment of earthquake hazards requires a characterization of the seismic sources that will produce ground motions of engineering significance at the site or area of interest. Seismic source characterization is concerned with three fundamental elements: (1) the identification, location, geometry, and rupture characteristics of significant sources of earthquakes; (2) the maximum size of these earthquakes (M_{max}); and (3) the rate at which they occur. For a deterministic earthquake scenario analysis, only the characterization of a single selected seismic source is required. Parameters needed

are fault location, geometry, and orientation; sense of slip; and M_{max}. No recurrence rate information is used in the scenario analysis.

In a probabilistic hazard assessment, all seismic sources that can generate significant ground shaking at a site, generally within a distance of 100–200 km (62–124 mi) in the western U.S., are characterized. For the map area, this larger study region is shown in Figure 1. Two general types of seismic sources were considered in the probabilistic hazard analysis: active or seismogenic faults and areal source zones or seismotectonic provinces.

The uncertainties in the seismic source parameters described below, which were sometimes large, were incorporated into the probabilistic seismic hazard analysis using a logic tree approach. In this procedure, values of the source parameters are represented by the branches of logic trees with weights that define the distribution of values. An example logic tree for a fault is shown in Figure 2. In general, three values for each parameter were weighted and used in the analysis. Statistical analyses indicate that a three-point distribution of 5th, 50th, and 95th percentiles weighted 0.185, 0.63, and 0.185 (rounded to 0.2, 0.6, and 0.2), respectively, is the best three-point discrete approximation of a continuous distribution (Keefer and Bodily 1983). Alternatively, they found that the 10th, 50th, and 90th percentiles weighted 0.3, 0.4, and 0.3, respectively, can be used when limited available data make it difficult to determine the extreme tails (i.e., the 5th and 95th percentiles) of a distribution. Note that the weights associated with the percentiles are not equivalent to probabilities for these values; they are just assigned weights to define the distribution. We generally applied these guidelines in developing distributions for many seismic source parameters (e.g., M_{max}, fault dip, slip rate, or recurrence) unless available data suggested it was inappropriate. Estimating the 5th, 95th, or even 50th percentiles is typically challenging and involves subjective judgment given limited available data.

The following discussion focuses on the seismic source characterization for the probabilistic hazard analysis. The single values used in the scenario ground-motion estimation are discussed in the section "Scenario ground motions." The source parameters for the significant faults in the study region and areal source zones were estimated and used in the probabilistic analysis. All seismic sources were assigned a range of maximum seismogenic depths of 12, 15, and 18 km (7.5, 9, and 11 mi), weighted 0.2, 0.6 and 0.2, respectively. This distribution of depths was primarily based on analyses of well-located earthquakes in the Rio Grande rift and incorporates the variability often observed (e.g., Sanford et al. 1991; Wong et al. 1995).

The study region spans several seismotectonic provinces, but lies primarily within the Rio Grande rift, a subprovince of the Basin and Range province. It also includes the Colorado Plateau, Rocky Mountains, and Great Plains province (Fig. 1). This analysis expands on our previous probabilistic hazard studies in the region (Wong et al. 1995, 1996a; Olig et al. 1998).

Quaternary faults. Machette (1998) discusses the importance of integrating Quaternary fault data into seismic hazard assessments in the Rio Grande rift, and we considered all known and suspected Quaternary faults within the study region (Fig. 3) for inclusion in our analyses. Fault parameters required in the probabilistic hazard analysis include: (1) rupture model including independent single plane, zone, segmented/unsegmented, and linked models; (2) probability of activity; (3) fault geometry including rupture length, rupture width, fault orientation, and sense of slip; (4) M_{max}; and (5) earthquake recurrence including both recurrence model and rates. These parameters are shown in Table 2 and discussed in general below.

To update and augment the input from

Text continued on p. 15

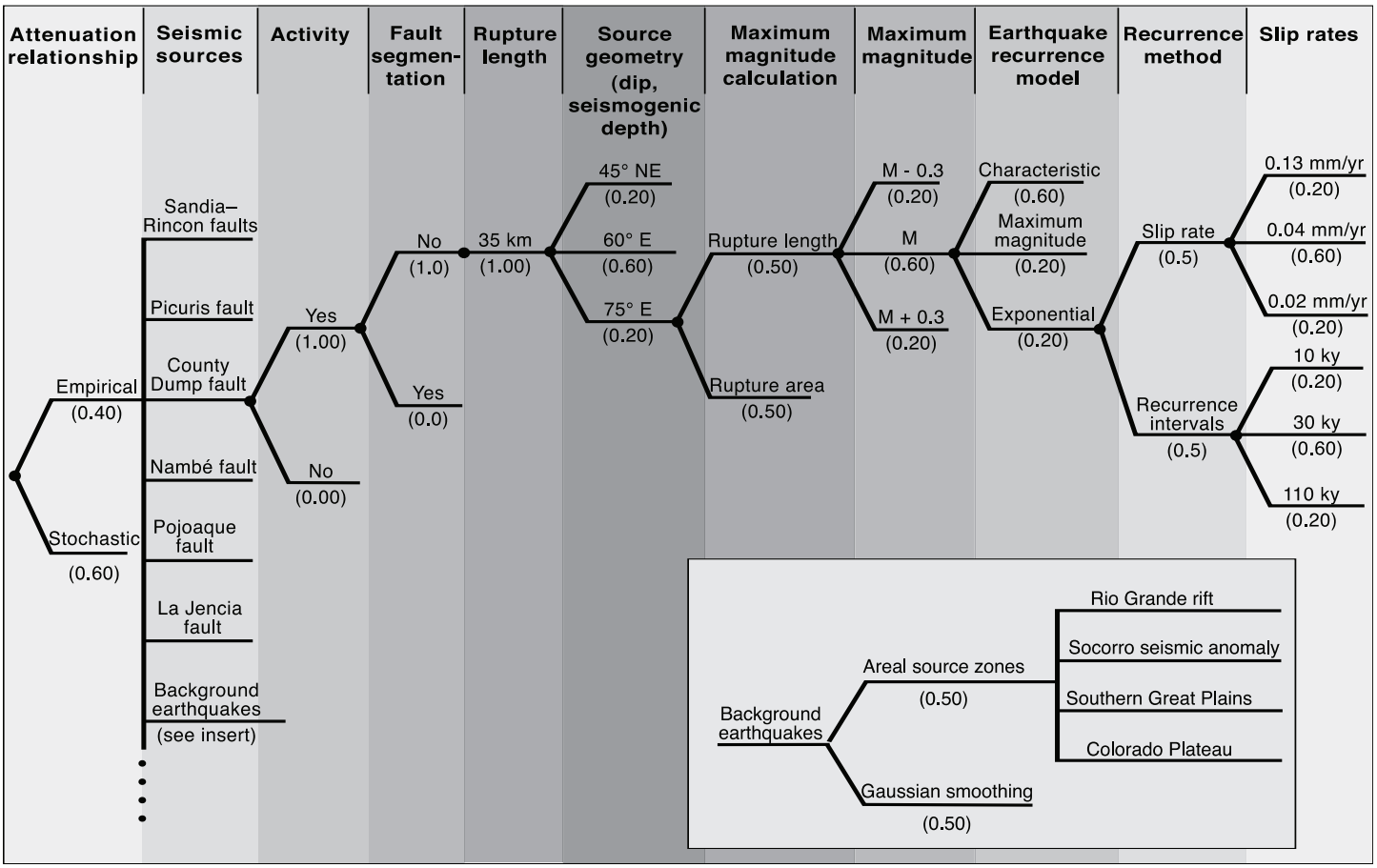

FIGURE 2—Example of a seismic hazard model logic tree. Weights for each parameter value are shown in parentheses.

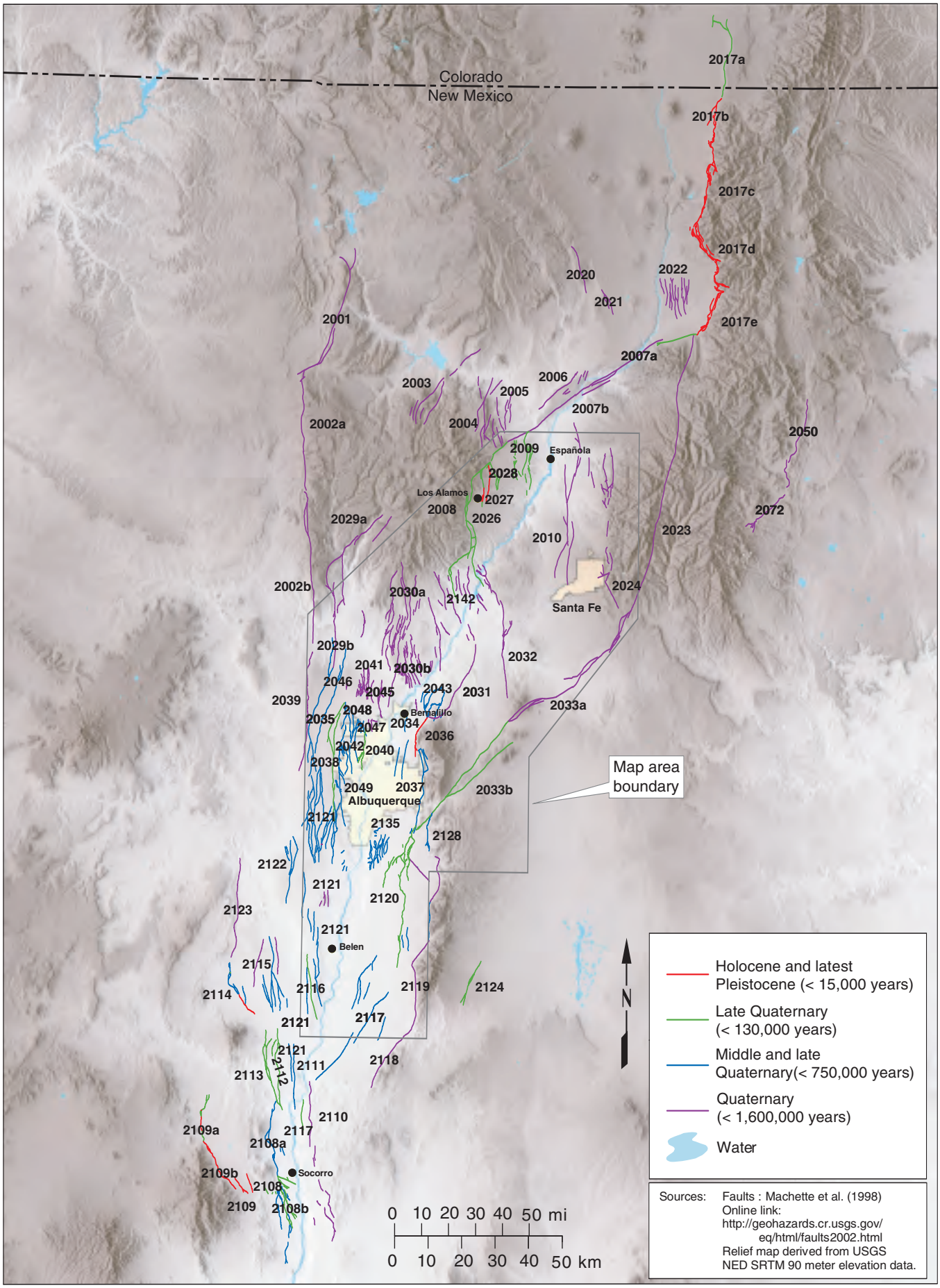

FIGURE 3—Quaternary faults included in the probabilistic seismic hazard analysis.

TABLE 2—Source parameters for Rio Grande rift faults.

Fault no.[1]	Fault name	Rupture model[2]	Maximum rupture length[3] (km)	Maximum magnitude[4] (M_w)	Dip[5] (degrees)	Approximate age of youngest activity[6]	Probability of activity[7]	Rate of activity[8] (mm/yr)
2001	Gallina fault	Independent (1.0)	39	6.7 (0.2) 7.0 (0.6) 7.3 (0.2)	45 E (0.2) 60 E (0.6) 75 E (0.2)	Quaternary?	0.5	0.005 (0.2) 0.02 (0.6) 0.2 (0.2)
2002	Nacimiento fault	Segmented (0.8)	N. section (2002a) 36	N. Section: 6.6 (0.2) 6.9 (0.6) 7.2 (0.2)	45 E (0.2) 60 E (0.6) 75 E (0.2)	N. Section – Quaternary	N. Section – 0.7	0.005 (0.2) 0.02 (0.6) 0.2 (0.2)
		Unsegmented (0.2)	S. Section (2002b) 45	S. Section: 6.7 (0.2) 7.0 (0.6) 7.3 (0.2)		S. Section – mid to late Pleistocene (possibly even Holocene)	S. Section – 1.0	
			Both – 82	Both: 7.0 (0.2) 7.3 (0.6) 7.6 (0.2)			Both – 1.0	
2003	Cañones fault	Independent (1.0)	29	6.5 (0.2) 6.8 (0.6) 7.1 (0.2)	45 SE (0.2) 60 SE (0.6) 75 SE (0.2)	Pliocene?	0.5	0.005 (0.2) 0.02 (0.6) 0.2 (0.2)
2004	Lobato Mesa fault zone	Independent (1.0)	22	6.4 (0.2) 6.7 (0.6) 7.0 (0.2)	45 W (0.2) 60 W (0.6) 75 W (0.2)	Quaternary	1.0	0.01 (0.2) 0.05 (0.6) 0.4 (0.2)
2005	La Cañada del Amagre fault zone	Independent (1.0)	12	6.1 (0.2) 6.4 (0.6) 6.7 (0.2)	60 E (0.3) 70 E (0.4) 80 E (0.3)	Plio-Pleistocene	0.5	0.02 (0.2) 0.1 (0.6) 0.85 (0.2)
2006	Black Mesa fault zone	Independent (1.0)	19	6.2 (0.2) 6.5 (0.6) 6.8 (0.2)	70 NW (0.3) 90 (0.4) 70 SE (0.3)	Quaternary?	0.5	0.005 (0.2) 0.02 (0.6) 0.2 (0.2)
2007	Embudo fault	Segmented (0.8)	Pilar (2007a) Section – 39	6.7 (0.2) 7.0 (0.6) 7.3 (0.2)	80 SE (0.3) 90 (0.4) 80 NW (0.3)	Pilar Section late Quaternary	1.0	0.02 (0.2) 0.09 (0.6) 0.8 (0.2)
			Hernandez (2007b) Section – 32	6.6 (0.2) 6.9 (0.6) 7.2 (0.2)		Hernandez Section Quaternary	0.8	
		Unsegmented (0.2)	Both - 65	6.9 (0.2) 7.2 (0.6) 7.5 (0.2)				
2008	Pajarito fault	Independent (1.0)	49	6.7 (0.2) 7.0 (0.6) 7.3 (0.2)	45 E (0.2) 60 E (0.6) 75 E (0.2)	Holocene	1.0	0.01 (0.1) 0.05 (0.2) 0.09 (0.4) 0.2 (0.2) 0.95 (0.1)
2009	Puye fault	Independent (1.0)	19	6.2 (0.2) 6.5 (0.6) 6.8 (0.2)	65 E (0.2) 75 E (0.5) 90 (0.3)	Mid to late Quaternary	1.0	0.007 (0.2) 0.03 (0.6) 0.25 (0.2)
2010	Pojoaque fault	Independent (1.0)	48	6.8 (0.2) 7.1 (0.6) 7.4 (0.2)	45 W (0.2) 60 W (0.6) 75 W (0.2)	Quaternary?	0.5	0.005 (0.2) 0.02 (0.6) 0.2 (0.2)

TABLE 2—Source parameters for Rio Grande rift faults, continued.

Fault no.[1]	Fault name	Rupture model[2]	Maximum rupture length[3] (km)	Maximum magnitude[4] (M_w)	Dip[5] (degrees)	Approximate age of youngest activity[6]	Probability of activity[7]	Rate of activity[8] (mm/yr)
2017	Southern Sangre de Cristo fault	Segmented (0.8)	Cañon & Hondo Sections (2017e & d) 33	6.5 (0.2) 6.8 (0.6) 7.1 (0.2)	45 W (0.2) 60 W (0.6) 75 W (0.2)	Latest Pleistocene to Holocene Except San Pedro Mesa is late Quaternary	1.0	0.06 (0.2) 0.12 (0.35) 0.17 (0.25) 0.29 (0.2)
			Questa & Urraca Sections (2017c & b) – 38	6.6 (0.2) 6.9 (0.6) 7.2 (0.2)				(Same for all sections)
			San Pedro Mesa Section (2017a) – 23	6.4 (0.2) 6.7 (0.6) 7.0 (0.2)				
		Unsegmented (0.2)	Unsegmented – 93	7.1 (0.2) 7.4 (0.6) 7.7 (0.2)				
2020	Las Tablas fault	Independent (1.0)	15	6.1 (0.2) 6.4 (0.6) 6.7 (0.2)	45 W (0.2) 60 W (0.6) 75 W (0.2)	Early Pleistocene?	0.5	0.002 (0.2) 0.03 (0.6) 0.2 (0.2)
2021	Stong fault	Independent (1.0)	8	5.8 (0.2) 6.1 (0.6) 6.4 (0.2)	45 E (0.2) 60 E (0.6) 75 E (0.2)	Early Pleistocene?	0.5	0.001 (0.2) 0.01 (0.6) 0.03 (0.2)
2022	Los Cordovas faults	Independent (1.0)	12	6.0 (0.2) 6.3 (0.6) 6.6 (0.2)	45 W (0.2) 60 W (0.6) 75 W (0.2)	Early Pleistocene	1.0	0.01 (0.2) 0.02 (0.6) 0.03 (0.2)
2023	Picuris–Pecos fault	Independent (1.0)	98	7.1 (0.2) 7.4 (0.6) 7.7 (0.2)	70 W (0.1) 80 W (0.4) 90 (0.5)	Quaternary?	0.5	0.01 (0.2) 0.05 (0.6) 0.4 (0.2)
2024	Nambé fault	Independent (1.0)	48	6.7 (0.2) 7.0 (0.6) 7.3 (0.2)	60 W (0.4) 90 (0.3) 60 E (0.3)	Quaternary?	0.1	0.005 (0.2) 0.02 (0.6) 0.2 (0.2)
2026	Rendija Canyon fault	Independent (1.0)	11	6.0 (0.2) 6.3 (0.6) 6.6 (0.2)	60 W (0.2) 75 W (0.5) 90 (0.3)	Holocene or latest Pleistocene	1.0	0.01 (0.3) 0.02 (0.4) 0.06 (0.2) 0.25 (0.1)
2027	Guaje Mountain fault	Independent (1.0)	11	6.0 (0.2) 6.3 (0.6) 6.6 (0.2)	60 W (0.2) 75 W (0.5) 90 (0.3)	Holocene	1.0	0.01 (0.7) 0.02 (0.2) 0.14 (0.1)
2028	Sawyer Canyon fault	Independent (1.0)	11	6.0 (0.2) 6.3 (0.6) 6.6 (0.2)	65 E (0.2) 75 E (0.5) 90 (0.3)	Late Quaternary	1.0	0.007 (0.2) 0.03 (0.6) 0.25 (0.2)
2029	Jemez–San Ysidro fault	Segmented (0.6)	Jemez (2029a)– 24	6.4 (0.2) 6.7 (0.6) 7.0 (0.2)	80 E (0.3) 90 (0.4) 80 W (0.3)	Quaternary	1.0	0.01 (0.2) 0.06 (0.6) 0.5 (0.2)
			San Ysidro (2029b)– 34	6.6 (0.2) 6.9 (0.6) 7.1 (0.2)	45 E (0.2) 60 E (0.6) 75 E (0.2)	Mid to late Quaternary		
		Unsegmented (0. 4)	48	6.7 (0.2) 7.0 (0.6) 7.3 (0.2)	60 E (0.5) 90 (0.5)			

TABLE 2—Source parameters for Rio Grande rift faults, continued.

Fault no.[1]	Fault name	Rupture model[2]	Maximum rupture length[3] (km)	Maximum magnitude[4] (M_w)	Dip[5] (degrees)	Approximate age of youngest activity[6]	Probability of activity[7]	Rate of activity[8] (mm/yr)
2030	San Felipe fault zone	Segmented (0.7)	Algodones (2030b) 43	6.7 (0.2) 7.0 (0.6) 7.3 (0.2)	50 E (0.3) 70 E (0.4) 90 (0.3)	Early Pleistocene	1.0	0.007 (0.2) 0.03 (0.6) 0.25 (0.2)
			Santa Ana (2030a) 33	6.5 (0.2) 6.8 (0.6) 7.1 (0.2)	50 W (0.3) 70 W (0.4) 90 (0.3)			0.01 (0.2) 0.05 (0.6) 0.4 (0.2)
		Unsegmented (0.3) (Zone)	43	6.7 (0.2) 7.0 (0.6) 7.3 (0.2)	60 E (0.3) 90 (0.4) 60 W (0.3)			0.01 (0.2) 0.05 (0.6) 0.4 (0.2)
2031	San Francisco fault	Independent (1.0)	30	6.5 (0.2) 6.8 (0.6) 7.1 (0.2)	45 W (0.2) 60 W (0.6) 75 W (0.2)	Early Pleistocene	1.0	0.01 (0.3) 0.07 (0.6) 0.58 (0.1)
2032	La Bajada fault	Independent (1.0)	40	6.6 (0.2) 6.9 (0.6) 7.2 (0.2)	45 W (0.2) 60 W (0.6) 75 W (0.2)	Early Pleistocene	1.0	0.02 (0.3) 0.09 (0.6) 0.8 (0.1)
2033	Tijeras–Cañoncito fault	Segmented (0.9)	Galisteo Section (2033a) 37	6.6 (0.2) 6.9 (0.6) 7.2 (0.2)	80 E (0.3) 90 (0.4) 80 W (0.3)	Quaternary?	0.5	0.02 (0.2) 0.09 (0.6) 0.8 (0.2)
			Canyon Section (2033b) 42	6.7 (0.2) 7.0 (0.6) 7.3 (0.2)		Late Quaternary	1.0	
		Unsegmented (0.1)	79	7.0 (0.2) 7.3 (0.6) 7.6 (0.2)			1.0	
2034, 2036, 2037, 2043	Bernalillo fault (2034) Sandia fault (2037) Rincon fault (2036) faults north of Placitas (2043)	Linked (0.4)	41	6.7 (0.2) 7.0 (0.6) 7.3 (0.2)	45 W (0.2) 60 W (0.6) 75 W (0.2)	Mid to late Quaternary	1.0	0.02 (0.2) 0.1 (0.6) 0.85 (0.2)
		Independent (0.6)	Sandia – 25	6.4 (0.2) 6.7 (0.6) 7.0 (0.2)		Mid to late Quaternary		0.01 (0.2) 0.05 (0.6) 0.4 (0.2)
			Rincon – 13	6.4 (0.2) 6.7 (0.6) 7.0 (0.2)		Holocene		0.02 (0.2) 0.1 (0.6) 0.85 (0.2)
			Placitas – 10	5.9 (0.2) 6.2 (0.6) 6.5 (0.2)		Mid to late Quaternary		0.01 (0.2) 0.04 (0.6) 0.3 (0.2)
			Bernalillo–10	5.9 (0.2) 6.2 (0.6) 6.5 (0.2)		Mid to late Quaternary		0.005 (0.2) 0.02 (0.6) 0.2 (0.2)
2035	Calabacillas fault	Independent (1.0)	40	6.6 (0.2) 6.9 (0.6) 7.2 (0.2)	45 E (0.2) 60 E (0.6) 75 E (0.2)	Mid to late Pleistocene	1.0	0.01 (0.2) 0.05 (0.6) 0.4 (0.2)
2038	County Dump fault	Independent (1.0)	35	6.6 (0.2) 6.9 (0.6) 7.2 (0.2)	45 E (0.2) 60 E (0.6) 75 E (0.2)	Late Quaternary	1.0	Recurrence (0.5): 10 ky (0.2) 30 ky (0.6) 110 ky (0.2)

TABLE 2—Source parameters for Rio Grande rift faults, continued.

Fault no.[1]	Fault name	Rupture model[2]	Maximum rupture length[3] (km)	Maximum magnitude[4] (M_w)	Dip[5] (degrees)	Approximate age of youngest activity[6]	Probability of activity[7]	Rate of activity[8] (mm/yr)
								Slip rate (0.5): 0.02 (0.2) 0.04 (0.6) 0.13 (0.2)
2039	Sand Hill fault	Independent (1.0)	36	6.3 (0.2) 6.6 (0.6) 6.9 (0.2)	45 E (0.2) 60 E (0.6) 75 E (0.2)	Early Pleistocene?	0.8	0.005 (0.2) 0.02 (0.6) 0.2 (0.2)
2040	East Paradise fault	Independent (1.0)	14	6.1 (0.2) 6.4 (0.6) 6.7 (0.2)	45 W (0.2) 60 W (0.6) 75 W (0.2)	Late Quaternary	1.0	0.002 (0.2) 0.01 (0.6) 0.09 (0.2)
2041, 2045, 2047	Zone of older intrabasin faults near northern margin of Albuquerque–Belen Basin (includes: Picuda Peak faults (2041) Loma Barbon faults (2045) Loma Colorado de Abajo faults (2047)	Zone (1.0)	19	6.3 (0.2) 6.6 (0.6) 6.9 (0.2)	60 E (0.2) 90 (0.5) 60 W (0.3)	Early Pleistocene	1.0	0.01 (0.2) 0.04 (0.6) 0.3 (0.2)
2042, 2048, 2049	Zone of younger intrabasin faults in central Albuquerque–Belen Basin (includes: West Paradise fault (2042) Star Heights faults (2048) Albuquerque volcanoes faults (2049)	Zone (1.0)	26	6.4 (0.2) 6.7 (0.6) 7.0 (0.2)	70 E (0.3) 90 (0.4) 70 W (0.3)	Mid to late Quaternary	1.0	0.01 (0.2) 0.04 (0.6) 0.3 (0.2)
2046	Zia fault	Independent (1.0)	32	6.5 (0.2) 6.8 (0.6) 7.1 (0.2)	45 E (0.2) 60 E (0.6) 75 E (0.2)	Mid to late Quaternary	1.0	0.01 (0.2) 0.04 (0.6) 0.3 (0.2)
2050	El Oro fault	Independent (1.0)	27	6.4 (0.2) 6.7 (0.6) 7.0 (0.2)	45 W (0.2) 60 W (0.6) 75 W (0.2)	Mid to late Quaternary	1.0	0.01 (0.2) 0.05 (0.6) 0.4 (0.2)
2059	Unnamed fault northeast of Longhorn Ranch	Independent (1.0)	10	5.9 (0.2) 6.2 (0.6) 6.5 (0.2)	60 W (0.5) 90 (0.5)	Quaternary ?	0.3	0.005 (0.3) 0.02 (0.6) 0.2 (0.1)
2072	Quebraditas fault zone	Independent (1.0)	15	6.1 (0.2) 6.4 (0.6) 6.7 (0.2)	45 W (0.2) 60 W (0.6) 75 W (0.2)	Mid to late Quaternary	1.0	0.01 (0.2) 0.05 (0.6) 0.4 (0.2)
2108a,b	Socorro Canyon fault zone	Independent (1.0)[9]	49	6.7 (0.2) 7.0 (0.6) 7.3 (0.2)	60 W (0.2) 90 (0.5) 60 E (0.3)	Mid to late Quaternary	1.0	0.01 (0.2) 0.05 (0.6) 0.4 (0.2)
2109a,b	La Jencia fault	Independent (1.0)[9]	34	6.6 (0.2) 6.9 (0.6) 7.2 (0.2)	45 E (0.2) 60 E (0.6) 75 E (0.2)	Late Quaternary for northern portion and latest Pleistocene to Holocene for southern portion	1.0	0.007 (0.2) 0.03 (0.6) 0.25 (0.2)
2110	West Joyita fault	Independent (1.0)	48	6.7 (0.2) 7.0 (0.6) 7.3 (0.2)	45 W (0.2) 60 W (0.6) 75 W (0.2)	Early Pleistocene	1.0	0.002 (0.2) 0.01 (0.6) 0.09 (0.2)
2111	Cliff fault	Independent (1.0)	19	6.3 (0.2) 6.6 (0.6)	45 W (0.2) 60 W (0.6)	Late Quaternary	1.0	0.01 (0.2) 0.05 (0.6)

TABLE 2—Source parameters for Rio Grande rift faults, continued.

Fault no.[1]	Fault name	Rupture model[2]	Maximum rupture length[3] (km)	Maximum magnitude[4] (M_w)	Dip[5] (degrees)	Approximate age of youngest activity[6]	Probability of activity[7]	Rate of activity[8] (mm/yr)
				6.9 (0.2)	75 W (0.2)			0.4 (0.2)
2112	Loma Blanca fault	Independent (1.0)	23	6.3 (0.2) 6.6 (0.6) 6.9 (0.2)	45 E (0.2) 60 E (0.6) 75 E (0.2)	Late Quaternary	1.0	0.02 (0.2) 0.06 (0.6) 0.5 (0.2)
2113	Loma Pelada fault	Independent (1.0)	24	6.4 (0.2) 6.7 (0.6) 7.0 (0.2)	45 E (0.2) 60 E (0.6) 75 E (0.2)	Late Quaternary	1.0	0.02 (0.2) 0.1 (0.6) 0.85 (0.2)
2114	Coyote Springs fault	Independent (1.0)	17	6.2 (0.2) 6.5 (0.6) 6.8 (0.2)	45 E (0.2) 60 E (0.6) 75 E (0.2)	Latest Pleistocene to Holocene	1.0	0.01 (0.2) 0.04 (0.6) 0.3 (0.2)
2115	Zone of intrabasin faults west of Rio Puerco	Zone (1.0)	22	6.3 (0.2) 6.6 (0.6) 6.9 (0.2)	60 W (0.3) 90 (0.4) 60 E (0.3)	Mid to late Quaternary	1.0	0.01 (0.2) 0.04 (0.6) 0.3 (0.2)
2116 & 2121 (southern group)	Southern zone of intrabasin faults on the Llano de Albuquerque (includes the Sabinal faults 2116)	Zone (1.0)	40	6.6 (0.2) 6.9 (0.6) 7.2 (0.2)	70 E (0.3) 90 (0.4) 70 W (0.3)	Mid to late Quaternary	1.0	0.01 (0.2) 0.04 (0.6) 0.3 (0.2)
2117 (northern group)	Zone of intrabasin faults on the Llano de Manzano	Zone (1.0)	17	6.2 (0.2) 6.5 (0.6) 6.8 (0.2)	60 W (0.3) 75 W (0.4) 90 (0.3)	Mid to late Quaternary	1.0	0.005 (0.2) 0.02 (0.6) 0.2 (0.2)
2117 (southern group)	Rift margin fault on the Llano de Manzano	Independent (1.0)	33	6.5 (0.2) 6.8 (0.6) 7.1 (0.2)	45 W (0.2) 60 W (0.6) 75 W (0.2)	Mid to late Quaternary	1.0	0.005 (0.2) 0.02 (0.6) 0.2 (0.2)
2118	Los Pinos fault	Independent (1.0)	18	6.2 (0.2) 6.5 (0.6) 6.8 (0.2)	45 W (0.2) 60 W (0.6) 75 W (0.2)	Quaternary?	0.5	0.002 (0.2) 0.01 (0.6) 0.09 (0.2)
2119	Manzano fault	Independent (1.0)	54	6.8 (0.2) 7.1 (0.6) 7.4 (0.2)	45 W (0.2) 60 W (0.6) 75 W (0.2)	Mid to late Quaternary	1.0	0.005 (0.2) 0.02 (0.6) 0.2 (0.2)
2120	Hubbell Spring fault	Independent (1.0)	43	6.7 (0.2) 7.0 (0.6) 7.3 (0.2)	45 W (0.2) 60 W (0.6) 75 W (0.2)	Late Pleistocene	1.0	0.02 (0.2) 0.1 (0.6) 0.85 (0.2)
2121 (northern group)	Northern zone of intrabasin faults on the Llano de Albuquerque	Zone (1.0)	35	6.6 (0.2) 6.9 (0.6) 7.2 (0.2)	70 E (0.3) 90 (0.4) 70 W (0.3)	Mid to late Quaternary	1.0	0.002 (0.2) 0.01 (0.6) 0.09 (0.2)
2122	Cat Mesa fault	Independent (1.0)	20	6.3 (0.2) 6.6 (0.6) 6.9 (0.2)	50 E (0.2) 75 E (0.6) 90 (0.2)	Middle Quaternary?	1.0	0.002 (0.2) 0.01 (0.6) 0.09 (0.2)
2123	Santa Fe fault	Independent (1.0)	30	6.5 (0.2) 6.8 (0.6) 7.1 (0.2)	45 E (0.2) 60 E (0.6) 75 E (0.2)	Quaternary?	0.7	0.002 (0.2) 0.01 (0.6) 0.09 (0.2)
2124	Faults west of Mountainair	Independent (1.0)	14	6.1 (0.2) 6.4 (0.6) 6.7 (0.2)	45 W (0.2) 60 W (0.6) 75 W (0.2)	Mid to late Quaternary	1.0	0.01 (0.2) 0.03 (0.6) 0.35 (0.2)
2128	Coyote	Independent (1.0)	11	6.0 (0.2)	45 W (0.2)	Mid to late Quaternary	1.0	0.01 (0.2)

TABLE 2—Source parameters for Rio Grande rift faults, continued.

Fault no.[1]	Fault name	Rupture model[2]	Maximum rupture length[3] (km)	Maximum magnitude[4] (M_w)	Dip[5] (degrees)	Approximate age of youngest activity[6]	Probability of activity[7]	Rate of activity[8] (mm/yr)
				6.3 (0.6) 6.6 (0.2)	60 W (0.6) 75 W (0.2)			0.04 (0.6) 0.3 (0.2)
2135	McCormick Ranch faults	Zone (1.0)	14	6.1 (0.2) 6.4 (0.6) 6.7 (0.2)	60 E (0.2) 90 (0.6) 60 W (0.2)	Mid to late Quaternary	1.0	0.005 (0.2) 0.02 (0.6) 0.2 (0.2)
2142	Faults near Cochiti Pueblo	Zone (1.0)	32	6.5 (0.2) 6.8 (0.6) 7.1 (0.2)	50 E (0.4) 90 (0.3) 50 W (0.3)	Pleistocene	1.0	0.01 (0.3) 0.06 (0.6) 0.5 (0.1)
Not applicable[10]	Palace-Pipeline	Independent (1.0)	27	6.4 (0.2) 6.7 (0.6) 7.0 (0.2)	55 W (0.2) 70 W (0.6) 85 W (0.2)	Pleistocene	1.0	0.005 (0.2) 0.02 (0.6) 0.2 (0.2)

[1]Fault number and nomenclature after Machette et al. (1998).

[2]Possible rupture models include: zones, independent single faults, segmented and unsegmented faults, and linked faults. Zones are modeled as random point sources within the zone boundary. Segmented and unsegmented faults allow for independent rupture for sections (or segments) of the fault. A linked model allows for coseismic rupture of faults, either along or across strike.

[3]Measured end to end (straight-line distance) on Machette et al. (1998).

[4]Preferred values estimated using the empirical relation of Wells and Coppersmith (1994) for all fault types. Estimates are based on displacement per event and/or maximum surface rupture length, depending on available data.

[5]Dips are averages for the seismogenic crust.

[6]Based on data in Machette et al. (1998). Categories are: Pliocene (1.6–5.3 Ma); Quaternary (<1.6 Ma); Pleistocene (10 ka–1.6 Ma); early Pleistocene (750 ka–1.6 Ma); late and middle Quaternary (<750 ka); late Quaternary (<130 ka); latest Pleistocene (10–15 ka); and Holocene (<10 ka).

[7]Probability of activity, p(a), considers the likelihood that a fault is an independent seismogenic structure and is still active within the modern stress field.

[8]Rates of fault activity are average net slip rates unless noted otherwise. For most faults, we assumed pure normal slip (100% dip slip), so these values were calculated from vertical slip rates (typically reported in the literature) by assuming the preferred fault dips. Recurrence models used in the analysis are not explicitly shown for each fault, but included characteristic, maximum-magnitude, and truncated-exponential, with weights depending on the type of seismic source and rupture model. For longer segmented faults, distributions are: characteristic – 0.6, maximum-magnitude – 0.3, and truncated-exponential – 0.1; except when only the recurrence approach was used and then characteristic was weighted 0.6 and maximum-magnitude was weighted 0.4. For shorter single independent faults, distributions are: characteristic – 0.6, maximum-magnitude – 0.2, truncated-exponential – 0.2. For faults modeled as zones, characteristic and truncated-exponential models are equally weighted (0.5).

[9]Although paleoseismic data indicate these faults are likely segmented (Machette et al., 1998), we assumed a single independent fault model for simplicity and because the faults are far away from the map area boundary.

[10]This newly recognized fault was not included in Machette et al. (1998), but is included here as mapped by Maldonado et al. (1999). It includes the westernmost traces of the McCormick Ranch faults as shown by Machette et al (1998), and so our modeling of the zone for the McCormick Ranch faults (2135) excluded these traces. As is the case with our modeling of many poorly understood intrabasin faults in the rift, we conservatively assumed these faults behave independently of each other for simplicity. Steeper dips were assumed for this relatively large intrabasin fault based on the cross section of Maldonado et al. (1999). Preferred slip rate based on scarps as high as 15m on the Sunport and Llano de Manzano surfaces that are estimated to be between 0.5 and 1.5 Ma (Maldonado et al., 1999). Slip-rate distribution developed similar to most other rift faults using the methodology of McCalpin (1995). See text for discussion.

our previous analyses we reviewed fault information from various sources, although most of the fault data used are from the Machette et al. (1998) compilation. We also contacted several geoscientists regarding their unpublished and ongoing work in the region. A total of 57 fault sources were characterized in this analysis. Figure 3 shows the location of all the fault sources, and Table 2 summarizes the fault source parameters used in our analysis. Fault nomenclature and numbers shown in Table 2 and in Figure 3 generally follow those used by Machette et al. (1998). Faults are listed in numerical order in Table 2.

We considered potential Quaternary fault sources as far away as 100 km (62 mi) from the map area boundary. Those faults that were judged to potentially contribute to the probabilistic hazard because of their activity, length, or proximity to the map area were included in the analysis. These included all longer (> 5 km [> 3 mi]) faults showing evidence for repeated Quaternary activity that are within 50 km (31 mi) of the map area boundary. We did not include faults ≤ 5 km (≤ 3 mi) long as they are considered to be accounted for by the areal source zones.

Where the data permit, we have attempted to consider and accommodate the structural variations that are potentially significant to the hazard analyses by including a variety of rupture behavior models and fault geometries in our source characterization (Table 2). All faults were modeled as zones or planes. Most faults show dominantly normal slip and are included as single independent (unsegmented) planar sources, unless the available data suggest otherwise. The rupture behavior of most of the faults in the region is poorly understood and is likely more complex than our simplifying assumptions, but we have attempted to address uncertainties that are significant to the hazard given our scope and the available data. Alternatives to the single-plane, independent fault model are segmented faults, linked faults, and zones of faults. Some faults show good evidence for being segmented (e.g., the Tijeras–Cañoncito fault), where relatively persistent segment boundaries have apparently confined prehistoric surface ruptures to particular parts of the faults. For other faults, the evidence is more ambiguous as to whether persistent rupture-segment boundaries exist (e.g., Jemez–San Ysidro fault). Whereas parts of potentially segmented faults may rupture independently of each other, potentially linked faults may experience coseismic rupture (either along or across strike). Ruptures of zones of faults are modeled as multiple, parallel, planar faults within the zone boundaries. Similar to the independent fault model, segmented and linked faults are modeled as planar sources extending throughout the seismogenic crust. Thus, fault dips for all of these (nonzone) rupture models are averages estimated over the extent of the seismogenic crust. For most typical range-bounding normal faults, preferred dips are assumed to be 60° unless noted otherwise (Table 2), such as for zones of intrabasin faults and faults showing dominantly strike-slip offset, which were assumed to be steeper.

In assigning probabilities of activity for each fault source, we considered both the likelihood that the fault is structurally capable of independently generating earthquakes, and the likelihood that it is still active within the modern stress field. We incorporated many factors in assessing these likelihoods, such as orientation in the modern stress field, fault geometry (length, continuity, and dip), relation to other faults, age of youngest movement, rates of activity, geomorphic expression, amount of cumulative offset, and any evidence for a nontectonic origin. Faults with definitive evidence for repeated Quaternary activity were generally considered to be active (seismogenic) and assigned probabilities of 1.0 (Table 2). Exceptions include faults that may be secondary and dependent on other faults, faults or fault features that may have a nonseismogenic origin, and faults that may be too short to independently generate earthquakes (≤ 10 km [≤ 6.2 mi]). The probability of activity for faults that do not show definitive evidence for repeated Quaternary activity was individually judged based on available data and the criteria explained above. Resulting values range from 0.1 to 1.0 (Table 2). Machette (1998) discusses the tendency to underestimate seismic hazards in areas of slow extension by not adequately including contributions from Quaternary faults. We believe that using the criteria of repeated Quaternary activity for judging probability of activity adequately addresses this issue, even for faults with recurrence intervals on the order of hundreds of thousands of years (e.g., Pitaycachi fault; Bull and Pearthree 1988) or faults that show evidence of temporal clustering and extreme variations in rates of activity (e.g., Caballo and La Jencia faults; Machette 1998).

M_{max} was estimated using the empirical relationships developed by Wells and Coppersmith (1994) for all types of faults as noted in the footnotes of Table 2. We considered three models for recurrence—truncated-exponential, maximum-magnitude, and characteristic—with weights depending on the source geometry and type of rupture model (Fig. 2). Observations of historical seismicity and paleoseismic investigations suggest that characteristic recurrence behavior is more likely for individual faults, whereas seismicity in fault zones best fits a truncated-exponential recurrence model (Schwartz and Coppersmith 1984; Youngs and Coppersmith 1985). Therefore, we generally favored the characteristic recurrence model for all planar (or curvilinear planar) fault sources (i.e., the independent, segmented, unsegmented, and linked fault models), but assigned equal weights to the truncated-exponential and characteristic recurrence models for zones of faults (see footnote 8 of Table 2; Fig. 2). We assigned a slightly higher weight to the maximum-magnitude recurrence model, an extreme variation of the characteristic model (Wesnousky 1986), for longer segmented faults (0.3 versus 0.2 for shorter independent faults, and 0 for fault zones). This was based on the idea that as faults develop and become longer and more continuous, their behavior may evolve to become less exponential and more characteristic.

With the exception of the County Dump fault, we used slip rates to characterize rates of fault activity as recurrence interval data are generally lacking (Table 2). We considered all available long-term (≤ 1.6 Ma) and intermediate-term (≤ 130 ka) data in developing slip-rate or recurrence distributions, but we preferred intermediate-term data whenever it was available. In addition to the time period, we also considered the type and quality of data in determining slip or recurrence rates. Whenever possible we attempted to calculate or adjust for along-strike average net slip rates. For example, we converted vertical slip rates to net slip rates for most faults by assuming 100% dip slip and the preferred fault dips. Variations of displacements along strike can significantly affect the calculation of slip rates (Wong and Olig 1998), but unfortunately very few faults have enough data to calculate average rates for the entire fault (e.g., Pajarito fault). More typically there are only a few data points for one or two sites along the fault (e.g., Hubbell Spring fault) or no fault-specific data at all (e.g., La Bajada fault). In the latter case, we assumed slip-rate distributions the same as a similar nearby structure, taking into account such factors as style of deformation, geomorphic expression, and age of youngest movement.

Unfortunately many Quaternary faults in the study area fall into the latter case or have only limited long-term slip-rate data (Machette et al. 1998). In his compilation of slip-rate data for Rio Grande rift faults, McCalpin (1995) generally found much higher intermediate-term (≤ 130 ka) rates than long-term rates (> 130 ka). This may be due to temporal clustering of earthquakes, inclusion of larger open-ended time periods in long-term rates, or other large inherent uncertainties in longer-term slip-rate data (Wong and Olig 1998).

To account for the possibility of temporal clustering and the underestimation of slip rates when large open-ended intervals are included in longer-term rates, we used an approach similar to that described by McCalpin (1995) to develop slip-rate distributions for faults where only limited or long-term data are available. We also used

this approach in our previous study of the Los Alamos National Laboratory, and additional discussion is provided in Wong et al. (1995, 1996a) and Wong and Olig (1998).

The method is based on an ergodic substitution of space for time so that the slip-rate data set for better-studied faults in the rift is used to determine a slip-rate distribution for a poorly known fault. This is accomplished by normalizing the slip rates for all the well-studied faults to a common factor relevant to the poorly known fault, such as the long-term rate. A cumulative frequency plot of these normalized rates then has the 50th percentile anchored at this long-term rate, and the plot shows the expected variation in rates assuming that the fault of interest behaves like other better-studied faults in the rift (Fig. 4). We then used this plot to determine 5th and 95th percentiles for our three-point slip-rate distribution as previously described. We recognize that this approach results in asymmetric distributions that are skewed toward higher rates and may not be appropriate for all faults, so we have modified slip-rate distributions whenever available geologic data indicate this is appropriate (e.g., Los Cordovas faults, San Francisco, and La Bajada faults). Despite the limitations and inherent assumptions, this approach does provide a way to systematically account for large uncertainties in slip rates for many Rio Grande rift faults. Sensitivity results for five sites show that these skewed slip distributions do have an effect on the mean probabilistic hazard, increasing it by 0.01–0.06 g for the 500-yr return period. This highlights the need for more detailed paleoseismic studies in the rift to better understand Quaternary fault behavior and temporal clustering of earthquakes in the region.

Background seismicity. The hazard from background (floating or random) earthquakes that are not associated with the known or mapped faults needs to be incorporated into the hazard analysis. Earthquake recurrence estimates in the study region and M_{max} estimates are required to assess the hazard from background earthquakes. In most of the western U.S., particularly the Basin and Range province, the M_{max} for earthquakes not associated with known faults usually ranges from **M** 6 to 6.5. Repeated events larger than these magnitudes probably produce recognizable fault- or fold-related features at the earth's surface (e.g., Doser 1985; dePolo 1994). In this study, we adopt a M_{max} value of **M** 6.5 ± 0.25.

In addition to the traditional approach of using areal source zones (assuming uniformly distributed seismicity), in this case, seismotectonic provinces, Gaussian smoothing (Frankel 1995) was used to address the hazard from background earthquakes in the probabilistic analysis. In this approach, we smoothed the historical background seismicity to incorporate a degree of stationarity, using a spatial window of 15 km (9.3 mi).

Using areal source zones, we defined three seismotectonic provinces in the study region: the Rio Grande rift, Southern Great Plains, and Colorado Plateau (Fig. 1). The Socorro seismic anomaly was also modeled as an areal source zone and differentiated from the rest of the Rio Grande rift because of its higher level of seismicity probably resulting from magmatic activity (Sanford et al. 1991).

We weighted the two approaches equally at 0.50. Both approaches were based on recently developed earthquake catalogs for New Mexico and bordering areas (Sanford et al. 2002). In these catalogs, epicentral locations and magnitudes for felt earthquakes (1869–1961) and for instrumentally recorded earthquakes (1962–1998) were reevaluated and, in a majority of cases, revised. A major effort was made to have all magnitudes in the catalogs based on a duration magnitude relation tied to M_L. The latter is equivalent to **M** in the magnitude range covered by the catalogs. Ranges in seismogenic crustal thickness were adopted for the background earthquakes based on the historical record (Wong et al. 1995).

The earthquake recurrence of the areal source zones was described by the truncated-exponential form of the Gutenberg–Richter relationship of $\log N = a - bM$. The recurrence relationships for the provinces were estimated using the maximum likelihood procedure developed by Weichert (1980) and the estimated completeness intervals for New Mexico (Lin 1999). In the computation of background seismicity recurrence, all events known to be associated with faults considered in the hazard analysis should be removed from the historical catalogs (Sanford et al. 2002). In this case, no such events could be identified, and thus no earthquakes were deleted.

Dependent events, such as aftershocks, foreshocks, and smaller events within an earthquake swarm were also identified and removed from the catalogs using the technique developed by Youngs et al. (2000). After adjusting the New Mexico catalogs (Sanford et al. 2002) for dependent events and completeness, 329 events in the range of M_L 2.0–5.8 remained from which to estimate the recurrence for the provinces (Fig. 1). The recurrence parameters are listed in Table 3.

Because of the limited duration of the historical catalogs (Sanford et al. 2002; 152 yrs), we incorporated uncertainties in the recurrence parameters for the background seismicity into the hazard analysis. We used three *b*-values: the best-estimate and ± 0.1 values, which were weighted 0.2, 0.6, and 0.2, respectively. An inspection of the resulting recurrence intervals for **M** 5 and 6 events was performed to weight the three *b*-values. The *a*-values were held fixed.

Geologic site-response categories and amplification factors

In order to quantify the site response of soil and unconsolidated sediments, a shear-wave velocity profile, depth to a reference rock datum, and dynamic degradation curves (both shear modulus reduction and damping) are required to define geologic site-response categories. Based on these site-response categories, frequency- and strain-dependent amplification factors can be computed as a function of input ground motions. It was obvious after initial efforts that there were insufficient geologic and geotechnical data to characterize the near-surface geology in the map area in sufficient detail to calculate region-specific amplification factors. Shear-wave velocity data for the map area were sparse with only six known measurement sites; five were located at alluvial sites in Albuquerque. Depth to a reference rock was known only in a few locations. Thus in the absence of region-specific data, three generic geologic site-response categories were defined: hard rock (A), soft rock (B), and firm/stiff soil (C). Lithologic units shown on the surficial geologic map of New Mexico (NMBGMR 2003) were assigned to one of the three site categories (Table 4) as shown in Figure 5 (page 23).

Based on the physical characterization used in the liquefaction susceptibility analysis by Kelson et al. (1999), it was apparent that the Quaternary alluvium along the Rio Grande shown on the state geologic map (NMBGMR 2003) as a single unit could have been further subdivided. Kelson et al. (1999) mapped areas within the Rio Grande valley underlain by saturated, unconsolidated sandy alluvium associated with the active floodplain of the Rio Grande. Because there were no other data of similar quality north and south of the area delineated by Kelson et al. (1999) and because there are insufficient data to differentiate in a definitive manner the site

TABLE 3—Earthquake recurrence parameters for seismotectonic provinces and area source zones.

Province	Number of earthquakes	*b*-value	*a*-value
Rio Grande rift	46	0.72 ± 0.08	-2.89
Southern Great Plains	105	0.76 ± 0.06	-3.22
Colorado Plateau	64	0.70 ± 0.07	-3.38
Socorro seismic anomaly	114	0.68 ± 0.05	-1.95

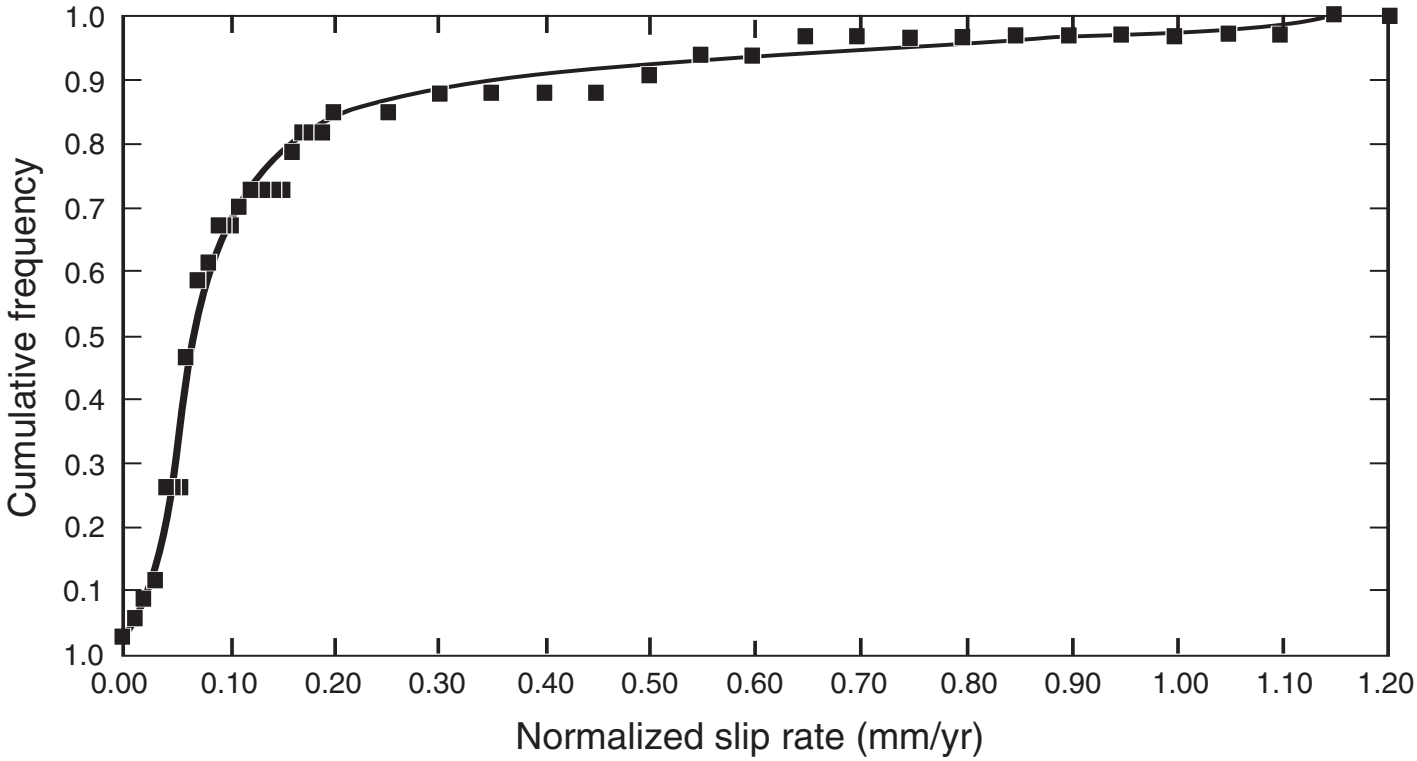

FIGURE 4—Slip rates normalized to 0.07 mm/yr for faults in the Rio Grande rift (from Wong and Olig 1998).

response between the stiff soil prevalent throughout the map area and the possibly softer soil along the Rio Grande, we included them both in the same site category (firm/stiff soil). The site response of the soft soils compared to the stiff soils is generally to damp out high-frequency ground motions (e.g., peak acceleration) and to amplify longer-period ground motions. This significant uncertainty should be noted in using the hazard maps.

Because region-specific amplification factors could not be computed due to a lack of data, factors based on the surficial geology in the San Francisco Bay area and Los Angeles, California, (Silva et al. 1999) were adopted (Table 5). These factors were developed using an equivalent-linear approach coupled with the stochastic numerical modeling technique (Silva et al. 1998). A comparison of lithologic descriptions for geologic units in the Rio Grande valley with similar units in California indicates that the California-based amplification factors are reasonable. To account for uncertainties in this approach, the amplification factors for broadly similar geologic categories in the San Francisco Bay area and Los Angeles area were combined and enveloped (Table 5). The California factors used in this study are also for a broad range in depths due to the lack of information on depths in the map area. The amplification factors are conservative because of these uncertainties.

Seismic attenuation characterization

To characterize the attenuation of ground motions in both the scenario and probabilistic analyses, we have used empirical attenuation relationships appropriate for soft rock sites in the western U.S. as well as the stochastic modeling approach (Silva et al. 1998). An important consideration in the selection of appropriate attenuation relationships is that the map area is located in the extensional tectonic regime of the Rio Grande rift where normal faulting predominates. The following empirical relationships were used: Abrahamson and Silva (1997) with normal faulting factors; Spudich et al. (1999), which was developed from an extensional earthquake strong-motion database; Sadigh et al. (1997); and Campbell (1997, 2000; Fig. 6). The latter two relationships are based primarily on California strong-motion data and were included to provide additional uncertainty. None of these relationships are specific to the Rio Grande rift due to the absence of strong-motion records in New Mexico. The relationships were weighted 0.40, 0.30, 0.15, and 0.15, respectively, based on our subjective judgment of the applicability of each relationship.

To compensate for the lack of region-specific attenuation relationships, the stochastic ground-motion modeling approach was used to develop relationships for the Rio Grande rift (Wong et al. 1996b; Fig. 6). Because all seismic sources were confined to the Rio Grande rift, with the exception of background seismicity to the west and east, the vast majority of raypaths from source to site are also confined to the rift. Thus, stochastic relationships were only developed for the Rio Grande rift. The point-source version of the stochastic methodology (Silva et al. 1998) was used to model earthquakes of **M** 5.5, 6.5, and 7.5 in the distance range of 1–400 km (0.62–250 mi). Uncertainties in stress drop, magnitude-dependent focal depths, crustal attenuation parameters Q_o and η, the near-surface attenuation parameter, kappa, and the shallow velocities at the top of the crustal model were included in the computations of the attenuation relationships through parametric variations (Wong et al. 1996b; Table 6). A range of magnitude-dependent stress drops appropriate for extensional regimes was used (Silva et al. 1997).

A P-wave velocity (V_P) crustal model consisting of three plane layers over a half-space derived from Prodehl and Lipman (1989) was used. The V_P values were converted to S-wave velocities (V_S) assuming a Poisson's ratio of 0.25. The model has crustal layer thicknesses of 4, 17, and 14 km (2.5, 10.5, and 8.7 mi) and the V_S values are 2.5, 3.5, and 3.7 km/sec (1.6, 2.2, and 2.3 mi/sec), respectively. The upper mantle half-space V_S is 4.5 km/sec (2.8 mi/sec). Inserted on top of this model is a generic western U.S. soft rock V_S profile developed from the database compiled by Pacific Engineering & Analysis.

Uncertainties in the regression of the simulated data are added to the modeling uncertainty to produce 16th, 50th (medi-

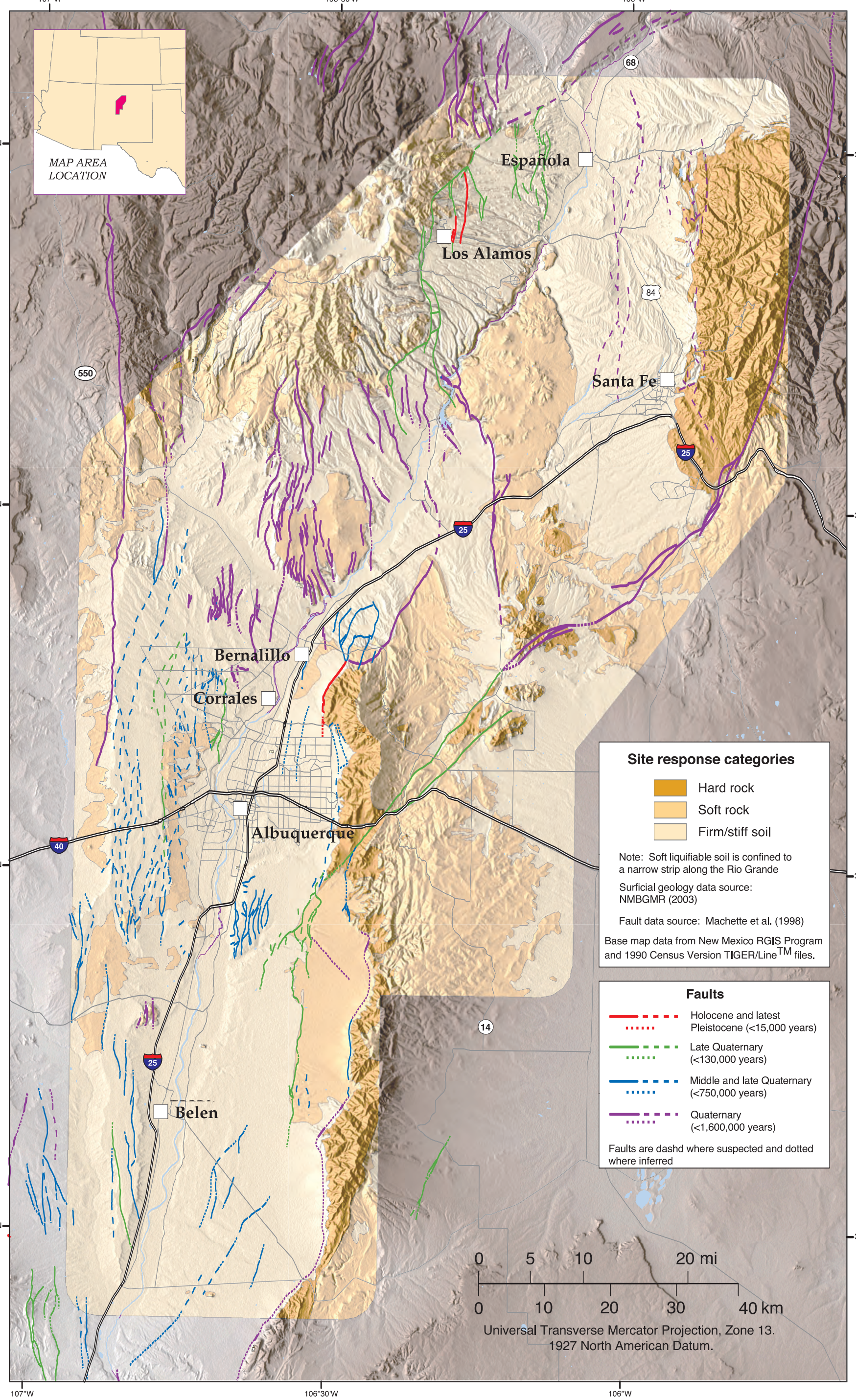

FIGURE 5—Geologic site-response categories for the map area. Potentially seismogenic faults are also shown.

TABLE 4—Classification of lithologic units of NMBGMR (2003) into geologic site-response categories: **A**—hard rock; **B**—soft rock; **C**—firm/stiff soil.

CATEGORY A

Unit	Surficial geology (NMBGMR 2003)	Lithology (NMBGMR 2003)
Ti	Intrusive rocks, undivided, Tertiary	Andesite and rhyolite
Yg	Plutonic rocks, Mesoproterozoic	Granite, gneiss
YXp	Plutonic rocks, Mesoproterozoic and Paleoproterozoic	Granite, gneiss, quartzite, schist, greenstone
Xps	Plutonic rocks, Paleoproterozoic	Gneiss, quartzite, schist, greenstone
Xs	Metasedimentary rocks, Paleoproterozoic	Metasediments, local high-grade quartzite-pelitic schist and amphibolite
Xvf	Metavolcanic, volcaniclastic rocks, Paleoproterozoic	High-grade felsic schist and gneiss of volcaniclastic and plutonic rocks
Xvm	Mafic metavolcanic and intrusive rocks, Paleoproterozoic	Mafic metavolcanic and intrusive rocks

CATEGORY B

Unit	Surficial geology (NMBGMR 2003)	Lithology (NMBGMR 2003)
Qb	Volcanic flows	Basaltic to andesitic lava flows
Qvr	Valles Rhyolite	Lava domes and flows of the Valles caldera
Qr	Silicic volcanic flows	Lower silicic lavas and volcaniclastic deposits of Valles caldera
QTt	Travertine	Deposited on Chinle Group, used Chinle value
QTb	Volcanic flows interbedded with Pleistocene and Pliocene sediments	Basalt, andesite, sediments
Tpb	Volcanic rocks, Pliocene	Volcanic vents and flows interbedded with Pliocene sediments
Tnb	Volcanic rocks, Neogene	Basalt and andesite flows, some Santa Fe Group interbedded
Tnr	Volcanic rocks, Neogene	Silicic to intermediate volcanic rocks, mostly Miocene
Tnv	Volcanic rocks, Neogene	Intermediate to silicic volcanic rocks of stratovolcanoes
Tvs	Sedimentary, volcaniclastic rocks, Oligocene and upper Eocene	Sedimentary rocks derived from andesite to intermediate volcanics, includes minor tuff breccias and flows
Tps	Sedimentary rocks, Paleogene	Sandstone, mudstone, conglomerate
Ku	Upper Cretaceous rocks, undivided	Sandstone, shale, local coal
Kmv	Mesaverde Group	Sandstone, local coal
Kms	Satan Tongue of the Mancos Shale	Shale
Kph	Hosta Tongue of the Point Lookout Sandstone	Sandstone
Kmm	Mulatto Tongue of the Mancos Shale	Shale
Kcc	Crevasse Canyon Formation	Sandstone, locally coal bearing
Kg	Gallup Sandstone	Sandstone
Km	Mancos Shale	Shale
Kml	Mancos Shale, lower part	Shale
Kd	Dakota Sandstone	Sandstone, shale, coal
J	Upper and Middle Jurassic rocks, undivided	Limestone, sandstone, mudstone, gypsum
Jm	Morrison Formation, Upper Jurassic	Limestone, sandstone, mudstone, gypsum
Jsr	San Rafael Group	Limestone, sandstone, mudstone, gypsum
TR	Triassic rocks, undivided	Continental red beds
TRc	Chinle Group, Upper Triassic	Mudstone, sandstone, minor conglomerate
P	Permian rocks, undivided	Sandstone, mudstone, gypsum
Pat	Artesia Group (may include Moenkopi Formation)	Shelf facies, sandstone
Pg	Glorieta Sandstone	High SiO_2 quartz sandstone
Psg	San Andres Limestone, Glorieta Sandstone	Limestone, sandstone
Py	Yeso Formation	Sandstone, siltstone, anhydrite, gypsum, halite, dolomite
Pa	Abo Formation	Sandstone, mudstone
Pb	Bursum Formation, Lower Permian	Shale, arkose, limestone
PIP	Permian and Pennsylvanian rocks, undivided	Limestone, sandstone, shale, mudstone, conglomerate
IP	Pennsylvanian rocks, undivided	Limestone, sandstone, shale, conglomerate, siltstone, mudstone
IPm	Madera Group	Limestone, sandstone, shale, conglomerate
IPs	Sandia Formation	Limestone, sandstone, shale, conglomerate
M	Mississippian rocks, undivided	Limestone, shale

CATEGORY C

Unit	Surficial geology (NMBGMR 2003)	Lithology (NMBGMR 2003)
Qa	Alluvium, upper to middle Quaternary	Alluvium (sand, gravel, silty clay)
Qa/QTs	Alluvium overlying upper Santa Fe Group	Soft alluvium, sandstone, pebble conglomerate
Ql	Landslide, colluvium	Landslide, colluvium
Ql/QTs	Landslide deposits over upper Santa Fe Group	Landslide, colluvium, sandstone, pebble conglomerate
Qe	Eolian deposits	Deposited on basalt and andesite flows
Qe/QTs	Eolian deposits over upper Santa Fe Group	Eolian sand, sandstone, pebble conglomerate
Qp	Piedmont alluvium, Quaternary	Alluvial deposits and fans
Qp/QTs	Piedmont alluvium over upper Santa Fe Group	Alluvial deposits, sandstone, pebble conglomerate
Qp/QTsf	Piedmont alluvium over undivided Santa Fe Group	Alluvial deposits, sandstone, pebble conglomerate, mudstone, siltstone, gravel
Qp/Tsf	Piedmont alluvium over middle and lower Santa Fe Group	Alluvial deposits, sandstone
Qoa	Alluvium, lower Quaternary–upper middle Pliocene	Alluvium, calcic soil, lacustrine, eolian, playa
Qbt	Bandelier Tuff	Rhyolite ash flows/falls, pumice, breccias, some welded tuff
QTs	Upper Santa Fe Group, Pleistocene–upper Miocene	Sandstone, pebble conglomerate
QTsf	Santa Fe Group, undivided, middle Pleistocene–upper Oligocene	Sandstone, pebble conglomerate, mudstone, siltstone, fanglomerate, arkose, gravel
Tsf	Middle to lower Santa Fe Group	Sandstone, mudstone, local ash beds, tuff, volcanic fanglomerate, andesite flows

TABLE 5—Amplification factors adopted from California site categories (Silva et al. 1999).

Rio Grande valley category	California category	Depth range (m)
A—Hard rock	Southern California granite	—
B—Soft rock	Tertiary rock	—
C—Firm/stiff soil	Quaternary/Tertiary sediment (QTs)	9–457

California category	Input rock motions PGA (g)	Amplification factors PGA (0.01 sec)	0.2 sec	1.0 sec
Q/T sediment	0.05	1.83	1.75	2.64
Q/T sediment	0.1	1.74	1.62	2.73
Q/T sediment	0.2	1.59	1.43	2.77
Q/T sediment	0.4	1.38	1.18	2.69
Q/T sediment	0.75	1.14	0.85	2.43
Q/T sediment	1.25	0.96	0.62	2.14
Tertiary rock	0.05	1.40	1.36	1.62
Tertiary rock	0.1	1.37	1.33	1.64
Tertiary rock	0.2	1.34	1.29	1.66
Tertiary rock	0.4	1.28	1.19	1.68
Tertiary rock	0.75	1.21	1.04	1.75
Tertiary rock	1.25	1.11	0.89	1.85

TABLE 6—Input parameters and standard errors used in the development of stochastic attenuation relationships.

Parameter	Values	Standard errors σ_{ln}
Magnitude (**M**)	5.5, 6.5, 7.5	—
Distance (km)	1, 5, 10, 20, 50, 75, 100, 200, 400	—
Magnitude-dependent point-source depth (km)[1]		
M 5.5	7.5 (4, 12)[2]	
M 6.5	7.5 (5, 10)[2]	0.6
M 7.5	7.5 (5, 10)[2]	
Magnitude-dependent stress drop (bars)[1]		
M 5.5	60	
M 6.5	45	0.7
M 7.5	36	
Crustal attenuation[1]		
Q_O	370	0.3
η	0.35	—
Kappa (sec)[1]	0.04	0.4

[1] Parameters randomly varied where σ_{ln} is based on observations.
[2] Upper- and lower-bound values.

an), and 84th percentile attenuation relationships. A total of 30 simulations were made for each magnitude and distance (total of 810), and the results fitted with a functional form that accommodates magnitude-dependent saturation and far-field fall-off (Fig. 6). The functional form is:

$$\ln Y = C_1 + C_2 \bullet \mathbf{M} + (C_6 + C_7 \bullet \mathbf{M}) \bullet \ln [R + \exp(C_4)] + C_{10} (\mathbf{M}-6)^2$$

where Y is the peak ground-motion parameter, R is rupture distance, and C_1 through C_{10} are coefficients fit to the data (Table 7). The parametric, modeling, and total uncertainties (vector sum of the first two) are also listed in Table 7.

The uncertainty in ground-motion attenuation was included in the probabilistic analysis by using the log-normal distribution about the median values as defined by the standard error associated with each attenuation relationship. Three standard deviations about the median value were included in the analysis.

Ground-motion calculations and map development

Ground motions were estimated for both the scenario and probabilistic hazard maps. Peak horizontal acceleration (defined at a frequency of 100 Hz) and spectral accelerations at periods of 0.2 and 1.0 sec were calculated using both empirical attenuation relationships and numerical modeling. The resulting ground-motion values were then displayed in map form using GIS.

Scenario ground motions

Ground motions were calculated for a **M** 7.0 scenario earthquake on the Sandia–Rincon faults. This scenario involved coseismic rupture of the Sandia, Rincon, and Placitas faults, resulting in a length of 41 km (25.5 mi). Although detailed trench studies are lacking, mapping and scarp-profiling suggest that the Rincon fault is one of the most active faults in the area (Connell 1995). The most recent surface-faulting event is indirectly estimated to have occurred about 2,000–5,000 yrs ago with an average displacement of approximately 2.3 m (Connell 1995). This is a much larger displacement than would be expected for this very short (≤ 11 km [6.8 mi] long) fault, and so we have considered the possibility that the Rincon fault may rupture with the Placitas fault to the north and the Sandia fault to the south, even though these faults appear to not have been as active during the Holocene (Connell 1995; Personius et al. 1999). Regardless, although one of the strands of the Sandia fault was recently trenched (McCalpin 2003), additional detailed study of these faults is definitely needed to better understand their behavior, particularly the Rincon fault.

The stochastic finite fault approach (Silva et al. 1998) was used to calculate scenario ground motions. This modeling explicitly incorporates the effects of the seismic source (fault geometry and dip, depth of rupture initiation, and sense of slip) and rupture propagation (e.g., directivity), which are particularly important at close distances to the fault. A slightly longer 48-km-long (29.8-mi-long) rupture of the Sandia, Rincon, and Placitas faults (actual length of 41 km [25.5 mi]) was modeled for the scenario earthquake to be consistent with a **M** 7.0 and static stress drops for extensional regimes. The rupture plane has a downdip width of 18.5 km (11.5 mi) and an assumed westward dip of 60°. A total of 30 simulations were made varying the slip distribution models and rupture initiation points. The same values of Q_o and η assumed for the stochastic attenuation relationships were used in the scenario calculations (Table 6). Scenario ground-motion values were calculated by assigning a 0.40 weight to the empirical values and 0.60 weight to the numerically modeled values.

Probabilistic ground motions

To calculate the probabilistic ground motions, a comprehensive Cornell hazard analysis using logic trees (Fig. 2) was performed employing the computer code HAZ32 developed by Norm Abrahamson. All known seismic sources that could generate strong ground shaking in the map area were incorporated into the probabilistic analysis (Table 2). Both empirical and stochastic attenuation relationships, weighted 0.40 and 0.60, respectively, were used in the analysis to calculate the ground-motion values. The mean probabilistic hazard was calculated at return periods of 500 and 2,500 yrs.

Map development

The ground-shaking maps were produced using a vector- and raster-based GIS program. Scenario and probabilistic ground motions on rock were calculated for the map area using a grid of points at 200-m (656-ft) spacings. Each grid point was assigned to a site-response category based on its location, and its surface ground motions were calculated by multiplying the rock ground motions by the appropriate amplification factors. The ground-motion values were then spatially smoothed with a circular window of 500-m (1,640-ft) radius so that no features smaller than this size were present on the maps. The intent was to avoid implying a greater level of resolution and/or accuracy than was possible given the limitations of the available geologic data. For each map, the peak or spectral acceleration values were

TABLE 7—Coefficients and uncertainties for the region-specific stochastic attenuation relationships. PGA = peak horizontal ground acceleration, PGV = peak horizontal ground velocity.

Freq. (Hz)	C_1	C_2	C_4	C_6	C_7	C_{10}	Parametric sigma	Model sigma	Total sigma
0.20	-17.22472	2.44981	1.70000	-1.03544	0.01279	-0.51566	0.3613	1.1358	1.1919
0.40	-10.73419	1.68876	1.90000	-1.35397	0.04419	-0.38758	0.4295	0.9297	1.0241
0.50	-8.96460	1.47553	2.00000	-1.45917	0.05301	-0.33937	0.4686	0.8642	0.9831
0.60	-7.31248	1.28631	2.10000	-1.58737	0.06510	-0.29251	0.5116	0.7946	0.9450
1.00	-4.08529	0.92389	2.30000	-1.86740	0.08859	-0.20784	0.4308	0.6627	0.7904
1.30	-2.50057	0.74621	2.40000	-2.05892	0.10578	-0.17010	0.4329	0.6613	0.7904
2.00	0.05253	0.51196	2.60000	-2.41788	0.13540	-0.12954	0.4955	0.5899	0.7704
2.50	1.18490	0.42780	2.70000	-2.59748	0.14795	-0.11909	0.4992	0.5648	0.7538
3.00	2.20721	0.35819	2.80000	-2.76841	0.15968	-0.11404	0.5443	0.5670	0.7860
4.00	3.51934	0.25432	2.90000	-3.03209	0.18055	-0.11417	0.5845	0.5377	0.7942
5.00	4.08219	0.19639	2.90000	-3.17053	0.19452	-0.12063	0.6461	0.5208	0.8298
6.00	5.04005	0.12394	3.00000	-3.36721	0.21014	-0.12663	0.6761	0.5098	0.8467
7.00	5.27193	0.10545	3.00000	-3.43444	0.21531	-0.13019	0.6601	0.5105	0.8345
8.00	5.52093	0.07676	3.00000	-3.49449	0.22148	-0.13097	0.6594	1.5187	0.8389
10.00	5.01164	0.09546	2.90000	-3.44776	0.22200	-0.14116	0.6544	0.4997	0.8234
12.00	4.95532	0.08979	2.90000	-3.47082	0.22619	-0.14907	0.6578	0.4890	0.8197
14.00	4.16492	0.14444	2.80000	-3.34611	0.21697	-0.15084	0.6487	0.4877	0.8116
16.00	3.97904	0.14958	2.80000	-3.32340	0.21631	-0.15216	0.6410	0.4916	0.8078
18.00	3.31182	0.18177	2.70000	-3.20509	0.20947	-0.14944	0.6183	0.4859	0.7864
20.00	3.11943	0.18940	2.70000	-3.17226	0.20760	-0.14780	0.6006	0.4891	0.7746
25.00	2.88759	0.18663	2.70000	-3.13176	0.20729	-0.14434	0.5852	0.4847	0.7599
31.00	2.30421	0.20856	2.60000	-3.02145	0.20184	-0.13701	0.5678	0.4793	0.7430
40.00	2.18322	0.20817	2.60000	-2.99676	0.20106	-0.13296	0.5550	0.4742	0.7300
50.00	2.08317	0.21493	2.60000	-2.97752	0.19949	-0.13167	0.5483	0.4768	0.7266
100.00	2.00764	0.21965	2.60000	-2.96370	0.19844	-0.13087	0.5438	0.4474	0.7236
PGA	2.05287	0.21292	2.60000	-2.96194	0.19820	-0.12802	0.5449	0.4774	0.7236
PGV	1.40332	0.75640	2.10000	-2.39660	0.17766	-0.18734	0.4256		

Note: C_3, C_5, C_8, and C_9 are zero.

color contoured by interpolation in intervals of 0.10 or 0.20 g.

Maps and results

In the following, we provide brief descriptions of the hazard maps that are shown as Figures 7 through 15. To assist those unfamiliar with the mapped ground-motion parameters, we show a correlation between peak horizontal ground acceleration and Modified Mercalli intensities developed by Wald et al. (1999) on both the maps and in Table 1.

M 7.0 Sandia–Rincon faults scenario maps

Figures 7 through 9 illustrate the ground shaking from the scenario earthquake. The probability of a **M** 7.0 event occurring on the Sandia–Rincon faults, assuming the rupture of the three linked faults, is probably on the order of 1 chance in several thousand to more than 1 chance in 10,000 on an annual basis. Examination of Figure 7 indicates that high-frequency ground motions, as characterized by peak horizontal acceleration, may exceed 0.8 g. The highest ground motions are in the hanging wall above the west-dipping Sandia–Rincon faults. This pattern is expected because the area lies directly over the fault rupture and because of amplification caused by the basin sediments. It should be noted that the effects of varying unconsolidated sediment thickness on amplification is not being exhibited on the maps because data were not available to incorporate it into the amplification factors. Only the general features of the potential ground motions are shown on the maps. Areas of thin unconsolidated sediments (tens of meters thick) will generally amplify high-frequency ground shaking, whereas thicker sequences will tend to dampen out high-frequency ground motions. Thus, differences in ground motions for a given site-response unit can be significant, but are not indicated on the maps.

The map for 0.2 sec spectral acceleration shows a somewhat different pattern of ground shaking (Fig. 8). The areas of greatest shaking correlate with areas on hard rock in the footwall (Sandia Mountains) east of the fault. This pattern suggests that 0.2 sec spectral accelerations are being damped out somewhat in the thick sequence of unconsolidated sediments in the basin of the hanging wall, relative to the hard rock. Note the high ground motions in the hanging wall south of Bernalillo, which happens to be a ridge of soft rock (Fig. 8). In contrast, Figure 9 illustrates dramatically the long-period amplifications of 1.0 sec spectral acceleration by the thick sediments in the basin as well as the hanging-wall effects. In the footwall, the ground motions are significantly lower on the hard rock of the Sandia Mountains (Fig. 9).

500-yr probabilistic maps

The probabilistic ground motions at a return period of 500 yrs (10% probability of exceedence in 50 yrs) are shown in Figures 10 through 12. Peak horizontal accelerations reach a maximum of 0.3 g. The areas of highest values are centered on Bernalillo northwest of Albuquerque and south of Belen in the southernmost corner of the map area. The Bernalillo area is comparatively high because of the concentration of faults and site amplification. The latter area lies within the seismically active Socorro seismic anomaly. The 0.2 sec spectral acceleration map shows more complexity because of a greater range of ground motions (Fig. 11). Site-response effects are also more prominent on this map. For example, the area of 0.3–0.4 g west of Santo Domingo Pueblo is underlain by soft rock (Fig. 5), and thus the amplification is lower there. The lowest hazard area is confined to the southern Sangre de Cristo Range, north and east of Santa Fe. There, both the Pojoaque and Nambé faults have low slip rates (~0.02 mm/yr; Table 2), and site amplification is assumed to be nonexistent because of the hard rock conditions. On the 1.0 sec spectral acceleration map, the higher long-period ground motions (> 0.2 g) correspond to areas of concentrated faulting in basins (Fig. 12). Thus site response and the concentration of seismic sources are both contributing to the hazard in these areas.

2,500-yr probabilistic maps

The hazard maps at a return period of 2,500 yrs (2% probability of exceedence in 50 yrs) are shown in Figures 13 through 15.

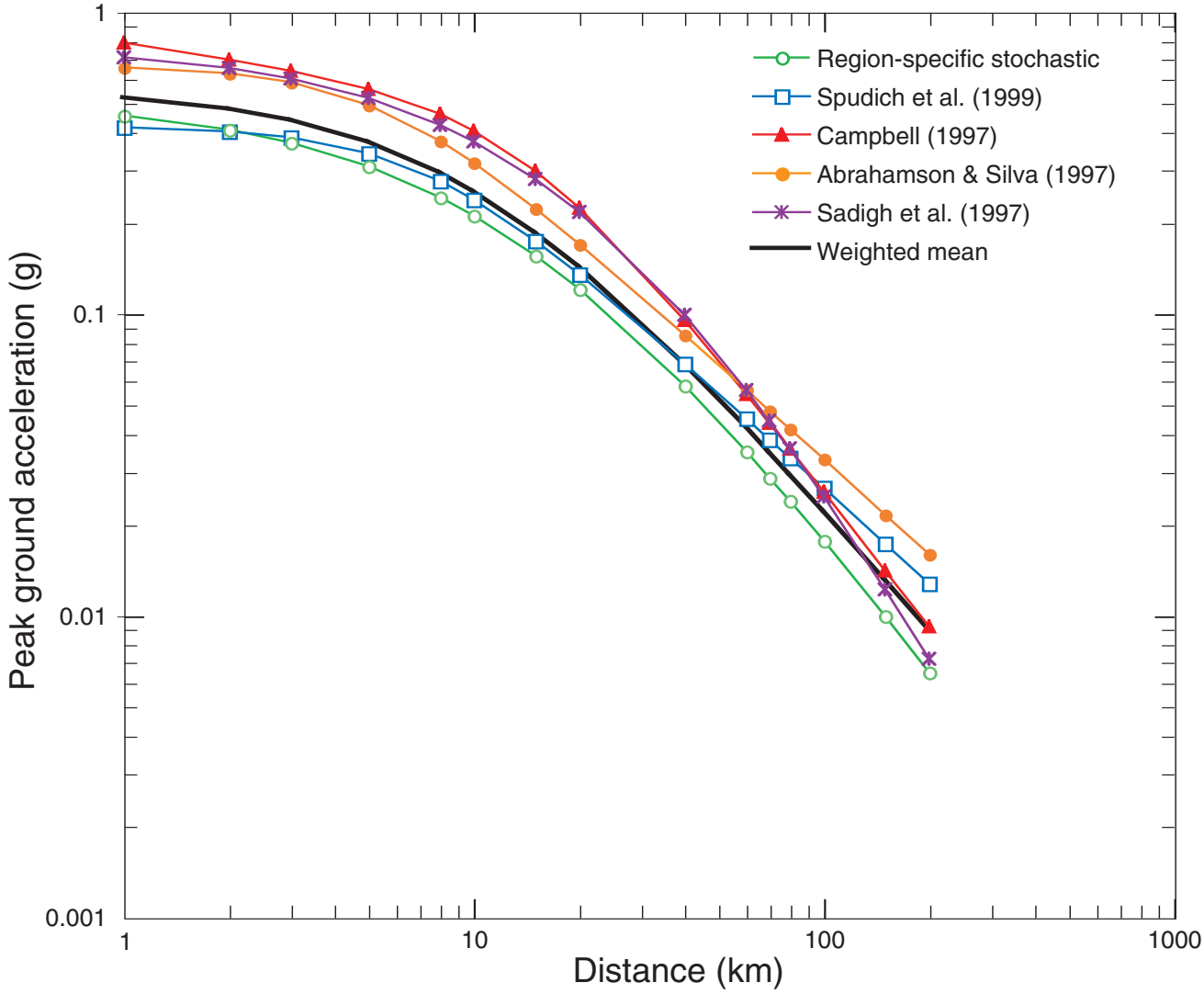

FIGURE 6—Comparison of rock attenuation relationships for **M** 7.0 used in this study.

The effect of the fault sources is emphasized on these maps because the recurrence intervals of large events occurring on them are approaching the return period of the map (2,500 yrs). Peak horizontal accelerations reach a maximum of 0.6 g. The areas of highest ground motions (> 0.4 g) coincide with faults with relatively high slip rates, such as the Hubbell Spring fault south of Albuquerque and the Pajarito fault system and Embudo fault near Los Alamos (Fig. 13). The patterns are similar for 0.2 and 1.0 sec spectral acceleration, with the former in particular highlighting areas of relatively active zones of faults north and southwest of Bernalillo (Figs. 14 and 15). Site-response effects from amplification of soils (Fig. 5) are also quite evident on all three maps.

Uncertainties

It must be emphasized that the ground-motion values displayed on these maps may have uncertainties as large as a factor of two or more. This is due to significant uncertainties associated with all three primary inputs into the hazard analysis: (1) seismic source characterization, (2) crustal attenuation, and (3) incorporation of site response. In terms of seismic source characterization, there have been few detailed paleoseismic investigations of New Mexico faults (Machette 1998), and thus for most of the faults characterized in this analysis, subjective judgment based on the available data has been used to estimate fault parameters.

One of the most perplexing aspects in evaluating the hazards is the surprisingly low level of historical seismicity in the map area and the absence of large magnitude (**M** > 6) events (Sanford et al. 1979, 1991). Extrapolations of the recurrence relationship of the seismicity record suggest a level that appears to contradict the available paleoseismic evidence (Machette 1998). Either the historical seismicity is reflecting a period of temporary quiescence in the rift, as first noted by Sanford et al. (1979), or possibly the current rate of extensional deformation across the rift is not as high as indicated by our long-term estimates of the slip rates for faults in the rift. In either case, we have explicitly included both possibilities in our analysis by incorporating a wide range of fault slip rates and a large uncertainty in the rate of background seismicity.

Possibly the greatest source of uncertainty is the estimation of rock ground motions through the use of attenuation relationships. These uncertainties reflect the current state-of-the-art in ground-motion estimation as indicated, for example, in the typical scatter of strong-motion data about a median attenuation relationship (see Abrahamson and Shedlock 1997). Because of the lack of subsurface information on the depth of unconsolidated sediments throughout the map area, the effects of the thickness of such units on ground motions also could not be explicitly accounted for in the amplification of the rock ground motions. Also topographic and basin effects on ground motions have not been

addressed in our analyses. Basin effects, which are long-period in nature (> 0.5 sec), may be significant in the Albuquerque Basin.

Comparison with national hazard maps

In 1996 the USGS released a "landmark" set of national hazard maps for earthquake ground shaking (Frankel et al. 1996), which was a significant improvement from previous maps they had developed. These maps were the result of the most comprehensive analyses of seismic sources and ground-motion attenuation ever undertaken on a national scale. The maps form the basis for the National Earthquake Hazards Reduction Program (NEHRP) Maximum Considered Earthquake maps, which are used in the International Building Code. The maps are for a uniform site condition in this case, NEHRP site class B/C (firm rock). The maps were updated in 2002 (Frankel et al. 2002).

For an exceedance probability of 2% in 50 yrs, the 2002 USGS maps show an elongated high in peak horizontal acceleration in New Mexico of 0.2–0.3 g centered on the Albuquerque–Belen–Santa Fe corridor for the B/C (firm rock) site condition. On our maps, areas underlain by a similar site condition, soft rock, are characterized by peak accelerations of 0.3–0.4 g. This is the opposite of what one would expect because of the low weight (0.2) the USGS assigned to the extensional attenuation relationship of Spudich et al. (1999) in comparison to the assignment of 0.88 weight for the empirical and regional-specific extensional relationships used in our calculations. The extensional relationships typically result in a 20% decrease in peak acceleration compared to the California relationships for the same magnitude and distance. Our ground motions, at least at peak acceleration, could be higher for a number of reasons, but the most significant is probably our more comprehensive treatment of Quaternary fault parameters with an emphasis on including uncertainties, particularly with regard to slip rates.

Summary

The purpose of this study was to quantify the ground shaking that might be experienced in the Albuquerque–Belen–Santa Fe corridor in terms of both a possible scenario earthquake and associated with specified exceedance probabilities relevant to building codes. Based on our analyses, the seismic hazard in the corridor can be viewed as moderate compared to other regions in the western U.S. The probabilistic hazard is significantly lower than in California and even in areas in the Basin and Range province such as the Salt Lake valley, Utah (Wong et al. 2002). However, the hazard is higher than other areas such as the parts of New Mexico to the west and east of the corridor and many other regions in the Basin and Range province such as southern Arizona.

The level of probabilistic hazard portrayed on the maps is controlled by the low level of historical seismicity (**M** ≤ 6), and by the comparatively low activity rates of the faults (slip rates generally less than 0.1 mm/yr). We caution again, however, that the historical seismicity record is often a poor indicator of the earthquake potential of a region. In addition, the geologic evidence is irrefutable that large-magnitude earthquakes (**M** ≥ 6.8) have occurred in the past and will undoubtedly occur in the future. Thus, although large earthquakes may be infrequent on a specific fault, the large number of faults in the corridor indicate that the apparent probability of a large earthquake occurring somewhere in the corridor is significant and increasing as further paleoseismic studies are being performed. The strong ground shaking from such an event, as illustrated by the **M** 7.0 Sandia–Rincon faults scenario, could be disastrous. The potential also exists for very large earthquakes occurring within the Rio Grande rift but outside the corridor, such as the 1887 **M** 7.4 Sonora earthquake, to impact population centers throughout New Mexico. Ground motions from any large earthquake can be quite severe because of the presence of alluvial sediments that blanket the Rio Grande valley and that can amplify ground shaking to very damaging levels.

Acknowledgments

This study was funded by the U.S. Geological Survey under National Earthquake Hazards Reduction Program Award 1434-HQ-97-GR-03018. The views and conclusions contained in this document are those of the authors and should not be interpreted as necessarily representing the official policies, either expressed or implied, of the U.S. government. Financial support was also provided by URS Corporation and Pacific Engineering & Analysis. We would like to thank the many individuals who provided us data, information, and assistance, including Michael Machette, Steve Personius, Kathleen Haller, Sean Connell, Keith Kelson, John Hawley, Jamie Gardner, Jim McCalpin, Bruce Harrison, Frank Pazzaglia, Missy Epps, Mike Rucker, Bob Reinke, Jeff Keaton, Jeff Unruh, Brian Stump, and Chuck Reynolds. Our thanks to Wendy Naugler, Fumiko Goss, Melinda Lee, Jane Love, Nancy Gilson, Leo Gabaldon, Rachel Griener, Doug Farson, and Marilyn Mackel for assisting in the preparation of this publication. The maps and report benefited greatly from reviews by Michael Machette and Jon Ake.

This project is supported by Grant #EMT-2004-GR-0103 awarded by the Federal Emergency Management Agency. This publication does not necessarily reflect FEMA's views.

References

Abrahamson, N. A., and Shedlock, K. M., 1997, Overview: Seismological Research Letters, v. 68, no. 1, pp. 9–23.

Abrahamson, N. A., and Silva, W. J., 1997, Empirical response spectral attenuation relations for shallow crustal earthquakes: Seismological Research Letters, v. 68, no. 1, pp. 94–127.

Baltz, E. H., 1978, Resumé of Rio Grande depression in north-central New Mexico; *in* Hawley, J. W. (comp.), Guidebook to Rio Grande rift in New Mexico and Colorado: New Mexico Bureau of Mines and Mineral Resources, Circular 163, pp. 210–228.

Bull, W. B., and Pearthree, P. A., 1988, Frequency and size of Quaternary surface ruptures of the Pitaycachi fault, northeastern Sonora, Mexico: Bulletin of the Seismological Society of America, v. 78, no. 2, pp. 956–978.

Campbell, K. W., 1997, Empirical near-source attenuation relationships for horizontal and vertical components of peak ground acceleration, peak ground velocity, and pseudo-absolute acceleration response spectra: Seismological Research Letters, v. 68, no. 1, pp. 154–179.

Campbell, K. W., 2000, Erratum to Campbell, 1997: Seismological Research Letters, v. 71, no. 3, pp. 352–354.

Chapin, C. E., 1979, Evolution of the Rio Grande rift—a summary; *in* Riecker, R. E. (ed.), Rio Grande rift–tectonics and magmatism: American Geophysical Union, pp. 1–5.

Connell, S. D., 1995, Quaternary geology and geomorphology of the Sandia Mountains piedmont, Bernalillo and Sandoval Counties, central New Mexico: Unpublished M.S. thesis, University of California, Riverside, 414 pp.

Davis, P. M., 1991, Continental rift structures and dynamics with reference to teleseismic studies of the Rio Grande and East African rifts; *in* Gangi, A. F. (ed.), World rift systems: Tectonophysics, v. 197, nos. 2–4, pp. 309–325.

dePolo, C. M., 1994, The maximum background earthquake for the Basin and Range province, western North America: Bulletin of the Seismological Society of America, v. 84, no. 2, pp. 466–472.

Doser, D. I., 1985, The 1983 Borah Peak, Idaho, and 1959 Hebgen Lake, Montana, earthquakes—models for normal fault earthquakes in the Intermountain seismic belt; *in* Stein, R. S., and Bucknam, R. C. (eds.), Proceedings of Workshop XXVIII on the Borah Peak, Idaho, earthquake: U.S. Geological Survey, Open-file Report 85-290, pp. 368–384.

Doser, D. I., and Yarwood, D. R., 1991, Strike-slip faulting in continental rifts—examples from Sabukia, East Africa (1928), and other regions; *in* Gangi, A. F. (ed.), World rift systems: Tectonophysics, v. 197, nos. 2–4, pp. 213–224.

DuBois, S. M., Smith, A. W., Nye, N. K., and Norwak, T. A., 1982, Arizona earthquakes, 1776–1980: Arizona Bureau of Geology and Mineral Technology, Bulletin 193, 456 pp.

Frankel, A., 1995, Mapping seismic hazard in the central and eastern United States: Seismological Research Letters, v. 66, no. 4, pp. 8–21.

Frankel, A., Mueller, C., Barnard, T., Perkins, D., Leyendecker, E. V., Dickman, N., Hanson, S., and Hopper, M., 1996, National seismic hazard maps—documentation June 1996: U.S. Geological Survey, Open-file Report 96-532, 110 pp.

Frankel, A., Petersen, M., Mueller, C., Haller, K., Wheeler, R., Leyendecker, E., Wesson, R., Harmsen, S., Cramer, C., Perkins, D., and Rukstales, K., 2002, Documentation for the 2002 update of the

national seismic hazard maps: U.S. Geological Survey, Open-file Report 02-420, 33 pp..
Keefer, D. I., and Bodily, S. E., 1983, Three-point approximations for continuous random variables: Management Science, v. 26, pp. 595–609.
Keller, G. R., Khan, M. A., Morgan, P., Wendlandt, R. F., Baldridge, W. S., Olsen, K. H., Prodehl, C., and Braile, L. W., 1991, A comparative study of the Rio Grande and Kenya rifts; *in* Gangi, A. F. (ed.), World rift systems: Tectonophysics, v. 197, nos. 2–4, pp. 355–371.
Kelson, K. I., Hitchcock, C. S., and Randolph, C .E., 1999, Liquefaction susceptibility in the inner Rio Grande valley near Albuquerque, New Mexico: Final technical report prepared for U.S. Geological Survey, 40 pp.
Lin, K. W., 1999, Probabilistic seismic hazard in New Mexico and bordering areas: Unpublished Ph.D. thesis, New Mexico Institute of Mining and Technology, Socorro, 194 pp.
Machette, M. N., 1987, Neotectonics of the Rio Grande rift, New Mexico (abs.): Geological Society of America, Abstracts with Programs, v. 19, no. 7, p. 754.
Machette, M. N., 1998, Contrasts between short- and long-term records of seismicity in the Rio Grande rift—important implications for seismic hazard assessments in areas of slow extension; *in* Lund, W. R. (ed.), Western States Seismic Policy Council Proceedings Volume, Basin and Range Province Seismic Hazards Summit: Utah Geological Survey, Miscellaneous Publication 98-2, pp. 84–95.
Machette, M. N., and Hawley, J. W., 1996, Neotectonics of the Rio Grande rift, New Mexico (abs.): Geological Society of America, Abstracts with Programs, v. 28, p. A-271.
Machette, M. N., Personius, S. F., Kelson, K. I., Haller, K. M., and Dart, R. L., 1998, Map and data for Quaternary faults and folds in New Mexico: U.S. Geological Survey, Open-file Report 98-521, 443 pp.
McCalpin, J. P., 1995, Frequency distribution of geologically determined slip rates for normal faults in the western United States: Bulletin of the Seismological Society of America, v. 85, no. 6, pp. 1867–1872.
McCalpin, J. P., 1998, Results from the seven-trench transect excavated in summer of 1997: Unpublished report for Los Alamos National Laboratory, GEO-HAZ Consulting, Inc., Estes Park, Colorado.
McCalpin, J. P., 2003, Paleoseismic investigations in the Rio Grande rift, USA, 1978–2003 (abs.): XVI INQUA Congress, Programs with Abstracts, Desert Research Institute, Reno, Nevada, p. 107.
Morgan, P., Seager, W. R., and Golombek, M. P., 1986, Cenozoic thermal, mechanical, and tectonic evolution of the Rio Grande rift: Journal of Geophysical Research, v. 91, no. B6, pp. 6263–6276.
Nakata, J. K., Wentworth, C. M., and Machette, M. N., 1982, Quaternary fault map of the Basin and Range and Rio Grande rift provinces western United States: U.S. Geological Survey, Open-file Report 82-579, 2 sheets, scale 1:2,500,000.
New Mexico Bureau of Geology and Mineral Resources (NMBGMR), 2003, Geological map of New Mexico, 1:500,000: New Mexico Bureau of Geology and Mineral Resources.
Olig, S., Youngs, R., and Wong, I., 1998, Probabilistic seismic hazard analysis for fault displacement at TA-3, LANL: Unpublished report prepared for the Los Alamos National Laboratory.
Olsen, K. H., Keller, G. R., and Stewart, J. N., 1979, Crustal structure along the Rio Grande rift from seismic refraction profiles; *in* Riecker, R. E. (ed.), Rio Grande rift—tectonics and magmatism: American Geophysical Union, pp. 127–143.
Personius, S. F., Machette, M. N., and Kelson, K. I ., 1999, Quaternary faults in the Albuquerque area—an update; *in* Pazzaglia, F. J., and Lucas, S. G. (eds.), Albuquerque geology: New Mexico Geological Society, Guidebook 50, pp. 189–200.
Personius, S. F., and Mahan, S. A., 2000, Paleoearthquake recurrence on the East Paradise fault zone, metropolitan Albuquerque, New Mexico: Bulletin of the Seismological Society of America, v. 90, no. 2, pp. 357–369.
Personius, S. F., and Mahan, S. A., 2003, Paleoearthquakes and eolian-dominated fault sedimentation along the Hubbell Spring fault zone near Albuquerque, New Mexico: Bulletin of the Seismological Society of America, v. 93, no. 3, pp. 1355–1369.
Prodehl, C., and Lipman, P. W., 1989, Crustal structure of the Rocky Mountain region; *in* Pakiser, L. C., and Mooney, W. D. (eds.), Geophysical framework of the continental United States: Geological Society of America, Memoir 172, pp. 249–284.
Reid, H. F., 1911, Remarkable earthquakes in central New Mexico in 1906 and 1907: Bulletin of the Seismological Society of America, v. 1, pp. 10–16.
Sadigh, K., Chang, C.-Y., Egan, J. A., Makdisi, F., and Youngs, R. R., 1997, Attenuation relationships for shallow crustal earthquakes based on California strong-motion data: Seismological Research Letters, v. 68, no. 1, pp. 180–189.
Sanford, A. R., Jaksha, L. H., and Cash, D. J., 1991, Seismicity of the Rio Grande rift in New Mexico; *in* Slemmons, D. B., Engdahl, E. R., Zoback, M. D., and Blackwell, D. D. (eds.), Neotectonics of North America: Geological Society of America, Decade Map, v. 1, pp. 229–244.
Sanford, A. R., Lin, K. W., Tsai, I. C., and Jaksha, L. H., 2002, Earthquake catalogs for New Mexico and bordering areas: 1869–1998: New Mexico Bureau of Geology and Mineral Resources, Circular 210, 101 pp.
Sanford, A. R., Olsen, K. H., and Jaksha, L. H., 1979, Seismicity of the Rio Grande rift; *in* Riecker, R. E. (ed.), Rio Grande rift—tectonics and magmatism: American Geophysical Union, pp. 145–168.
Schwartz, D. P., and Coppersmith, K. J., 1984, Fault behavior and characteristic earthquakes—examples from the Wasatch and San Andreas fault zones: Journal of Geophysical Research, v. 89, no. 7, pp. 5681–5698.
Silva, W. J., Abrahamson, N. A., Toro, G., and Constantino, C., 1997, Description and validation of the stochastic ground-motion model: Unpublished report prepared for the Brookhaven National Laboratory.
Silva, W. J., Li, S., Darragh, R., and Gregor, N., 1999, Surface geology based strong-motion amplification factors for the San Francisco and Los Angeles area: Unpublished report prepared for PEARL by Pacific Engineering & Analysis.
Silva, W. J., Wong, I. G., and Darragh, R. B., 1998, Engineering characterization of earthquake strong ground motions in the Pacific Northwest; *in* Rogers, A. M., Walsh, T. J., Kockleman, W. J., and Priest, G. R. (eds.), Assessing earthquake hazards and reducing risk in the Pacific Northwest: U.S. Geological Survey, Professional Paper 1560, v. 2, pp. 313–324.
Spudich, P., Joyner, W. B., Lindh, A. G., Boore, D. M., Margaris, B. M., and Fletcher, J. B., 1999, SEA99—a revised ground-motion prediction relation for use in extensional tectonic regimes: Bulletin of the Seismological Society of America, v. 89, no. 5, pp. 1156–1170.
Suter, M., and Contreras, J., 2002, Active tectonics of northeastern Sonora, Mexico (Southern Basin and Range province) and the 3 May 1887 M_W 7.4 earthquake: Bulletin of the Seismological Society of America, v. 92, no. 2, pp. 581–589.
Wald, D. J., Quitoriano, V., Heaton, T. H., and Kanomori, H., 1999, Relationships between peak ground acceleration, peak ground velocity, and Modified Mercalli intensity in California: Earthquake Spectra, v. 15, pp. 557–564.
Weichert, D. H., 1980, Estimation of the earthquake recurrence parameters for unequal observation periods for different magnitudes: Bulletin of the Seismological Society of America, v. 70, no. 4, pp. 1337–1346.
Wells, D., and Coppersmith, K. J., 1994, New empirical relationships among earthquake magnitude, rupture length, and fault displacement: Bulletin of the Seismological Society of America, v. 84, no. 4, pp. 974–1002.
Wesnousky, S. G., 1986, Earthquakes, Quaternary faults, and seismic hazard in California: Journal of Geophysical Research, v. 91, no. 12, pp. 12,587–12,631.
Wong, I., Kelson, K., Olig, S., Bott, J., Green, R., Kolbe, T., Hemphill-Haley, M., Gardner, J., Reneau, S., and Silva, W., 1996a, Earthquake potential and ground-shaking hazard at the Los Alamos National Laboratory; *in* Goff, F., Kues, B., Rogers, M. A., McFadden, L. D., and Gardner, J. (eds.), The Jemez Mountains region: New Mexico Geological Society, Guidebook 47, pp. 143–151.
Wong, I., Kelson, K., Olig, S., Kolbe, T., Hemphill-Haley, M., Bott, J., Green, R., Kanakari, H., Sawyer, J., Silva, W., Stark, C., Haraden, C., Fenton, C., Unruh, J., Gardner, J., Reneau, S., and House, L., 1995, seismic hazard evaluation of the Los Alamos National Laboratory: Final report prepared for the Los Alamos National Laboratory and the U.S. Department of Energy, 3 volumes.
Wong, I. G., and Olig, S. S., 1998, Seismic hazards in the Basin and Range province—perspectives from probabilistic analyses; *in* Lund, W. R. (ed.), Western States Seismic Policy Council Proceedings Volume, Basin and Range Province Seismic Hazards Summit: Utah Geological Survey, Miscellaneous Publication 98-2, pp. 110–127.
Wong, I., Silva, W., Olig, S., Thomas, P., Wright, D., Ashland, F., Gregor, N., Pechmann, J., Dober, M., Christenson, G., and Gerth, R., 2002, Earthquake scenario and probabilistic ground-shaking maps for the Salt Lake City, Utah, metropolitan area: Utah Geological Survey, Miscellaneous Publication MP-02-05, 50 pp.
Wong, I. G., Silva, W. J., Youngs, R. R., and Stark, C. L., 1996b, Numerical earthquake ground-motion modeling and its use in microzonation: Proceedings, 11th World Conference on Earthquake Engineering, Pergamon (CD-Rom).
Youngs, R. R., and Coppersmith, K. J., 1985, Implications of fault slip rates and earthquake recurrence models to probabilistic seismic hazard estimates: Bulletin of the Seismological Society of America, v. 75, no. 4, pp. 939–965.
Youngs, R. R., Swan, F. H., Power, M. S., Schwartz, D. P., and Green, R. K., 2000, Probabilistic analysis of earthquake ground-shaking hazard along the Wasatch Front, Utah; *in* Gori, P. L., and Hays, W. W. (eds.), Assessment of regional earthquake hazards and risk along the Wasatch Front, Utah: U.S. Geological Survey, Professional Paper 1500-K-R, pp. M1–M74.

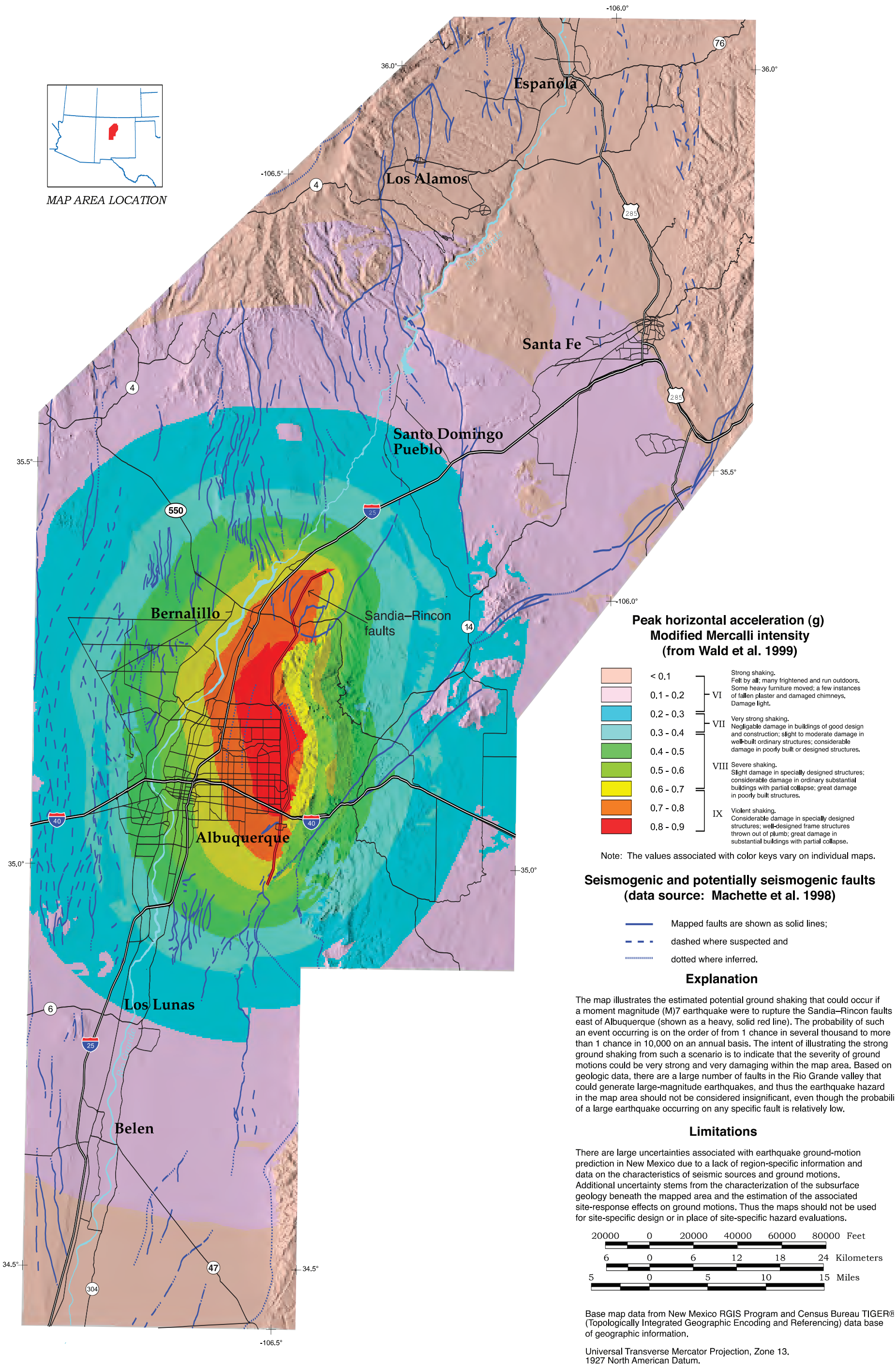

FIGURE 7—Earthquake scenario ground-shaking map for the Albuquerque–Belen–Santa Fe corridor, Sandia–Rincon faults **M** 7.0 earthquake, peak horizontal acceleration at the ground surface.

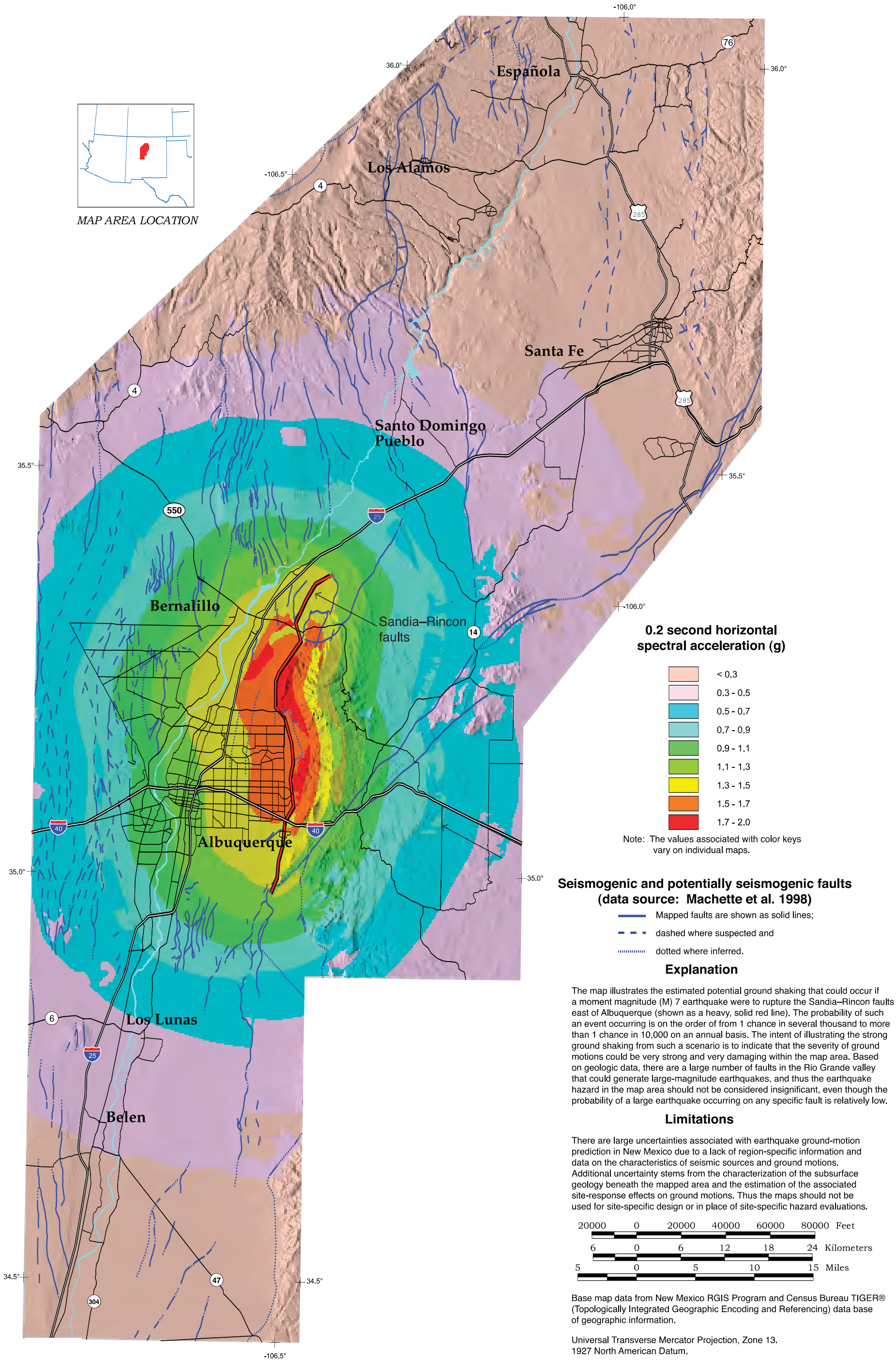

FIGURE 8—Earthquake scenario ground-shaking map for the Albuquerque–Belen–Santa Fe corridor, Sandia–Rincon faults **M** 7.0 earthquake, 0.2 sec horizontal spectral acceleration at the ground surface.

MAP AREA LOCATION

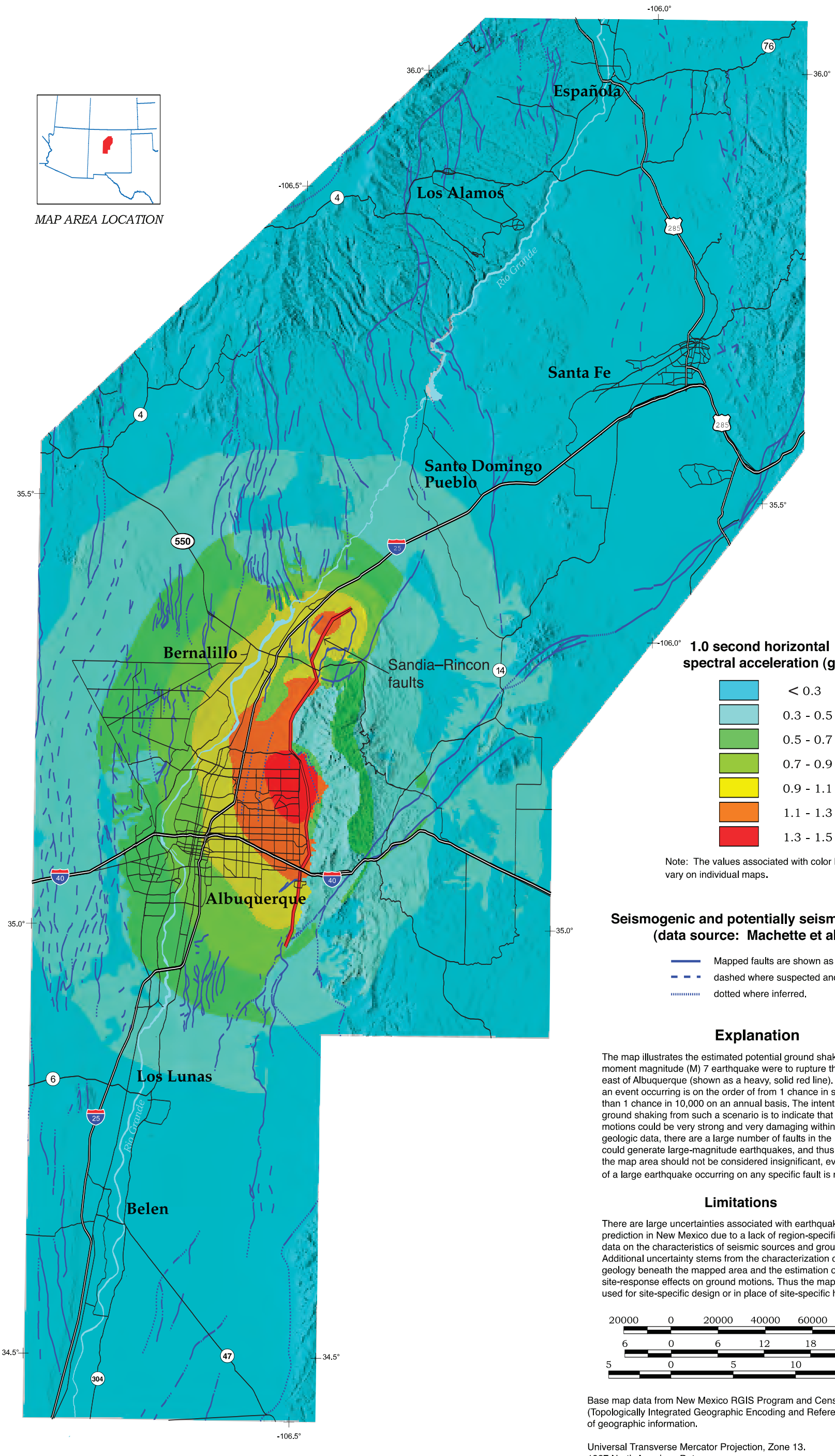

FIGURE 9—Earthquake scenario ground-shaking map for the Albuquerque–Belen–Santa Fe corridor, Sandia–Rincon faults **M** 7.0 earthquake, 1.0 sec horizontal spectral acceleration at the ground surface.

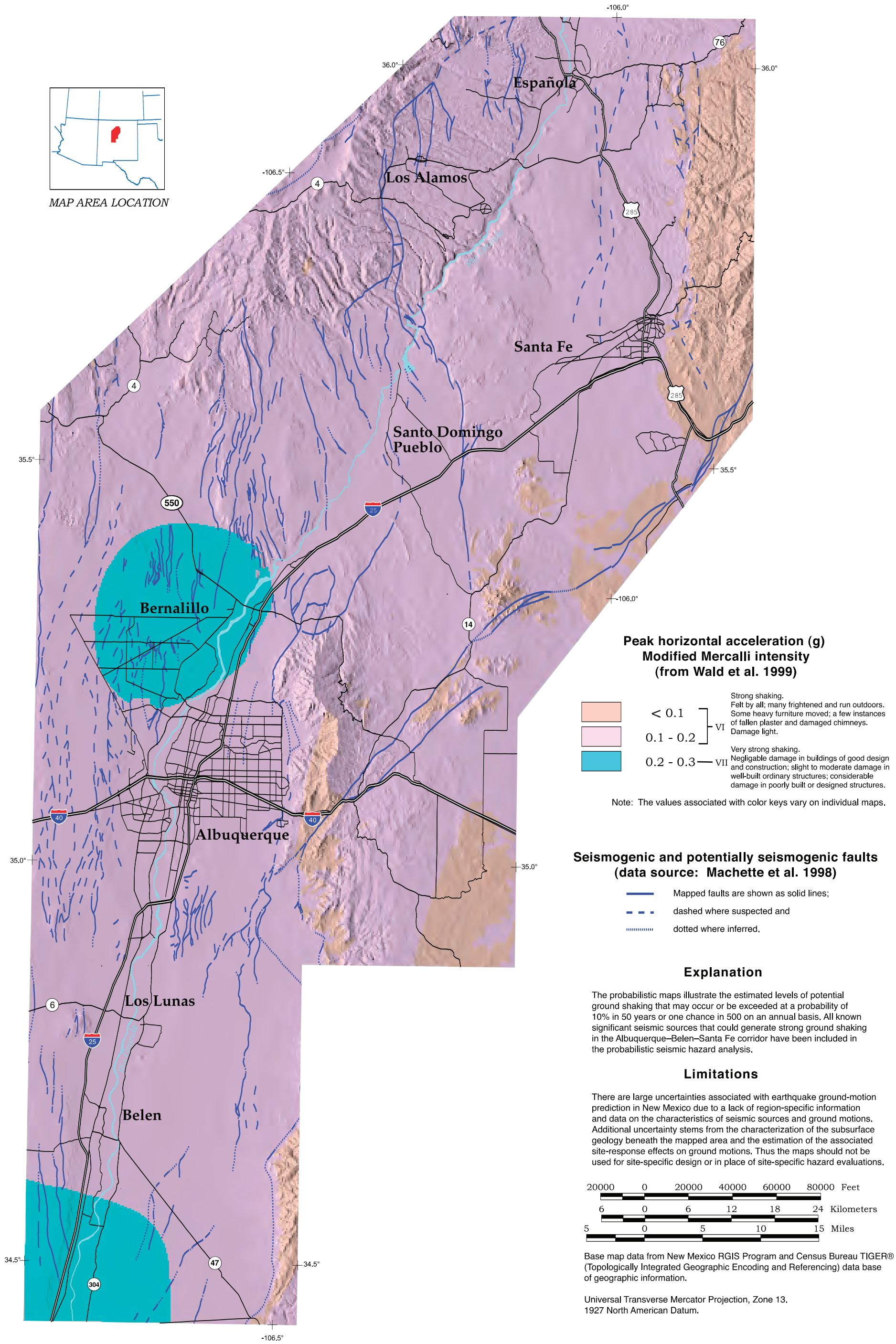

FIGURE 10—Probabilistic earthquake ground-shaking map for the Albuquerque–Belen–Santa Fe corridor, 10% probability of exceedance in 50 yrs, peak horizontal acceleration at the ground surface.

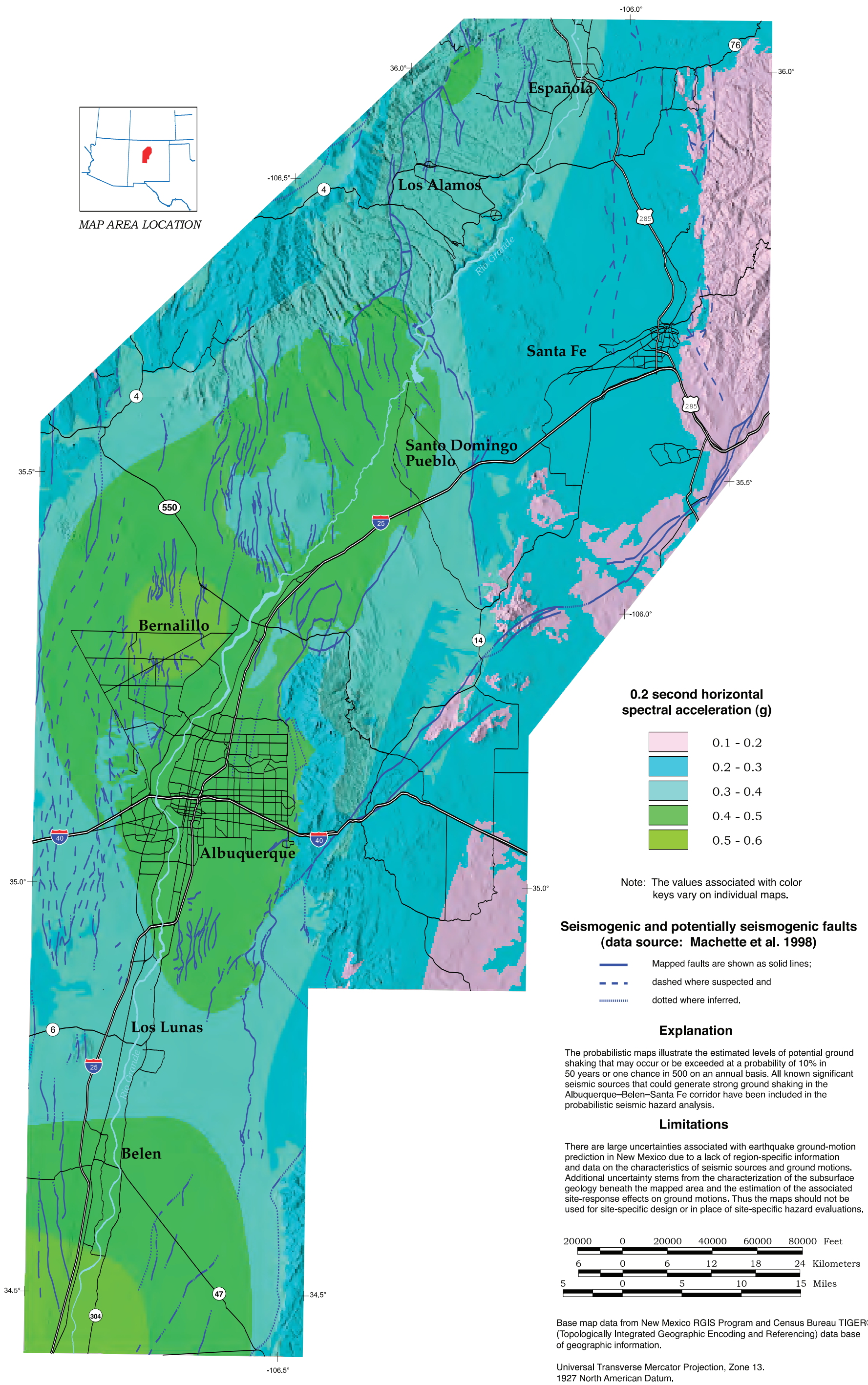

FIGURE 11—Probabilistic earthquake ground-shaking map for the Albuquerque–Belen–Santa Fe corridor, 10% probability of exceedance in 50 yrs, 0.2 sec horizontal spectral acceleration at the ground surface.

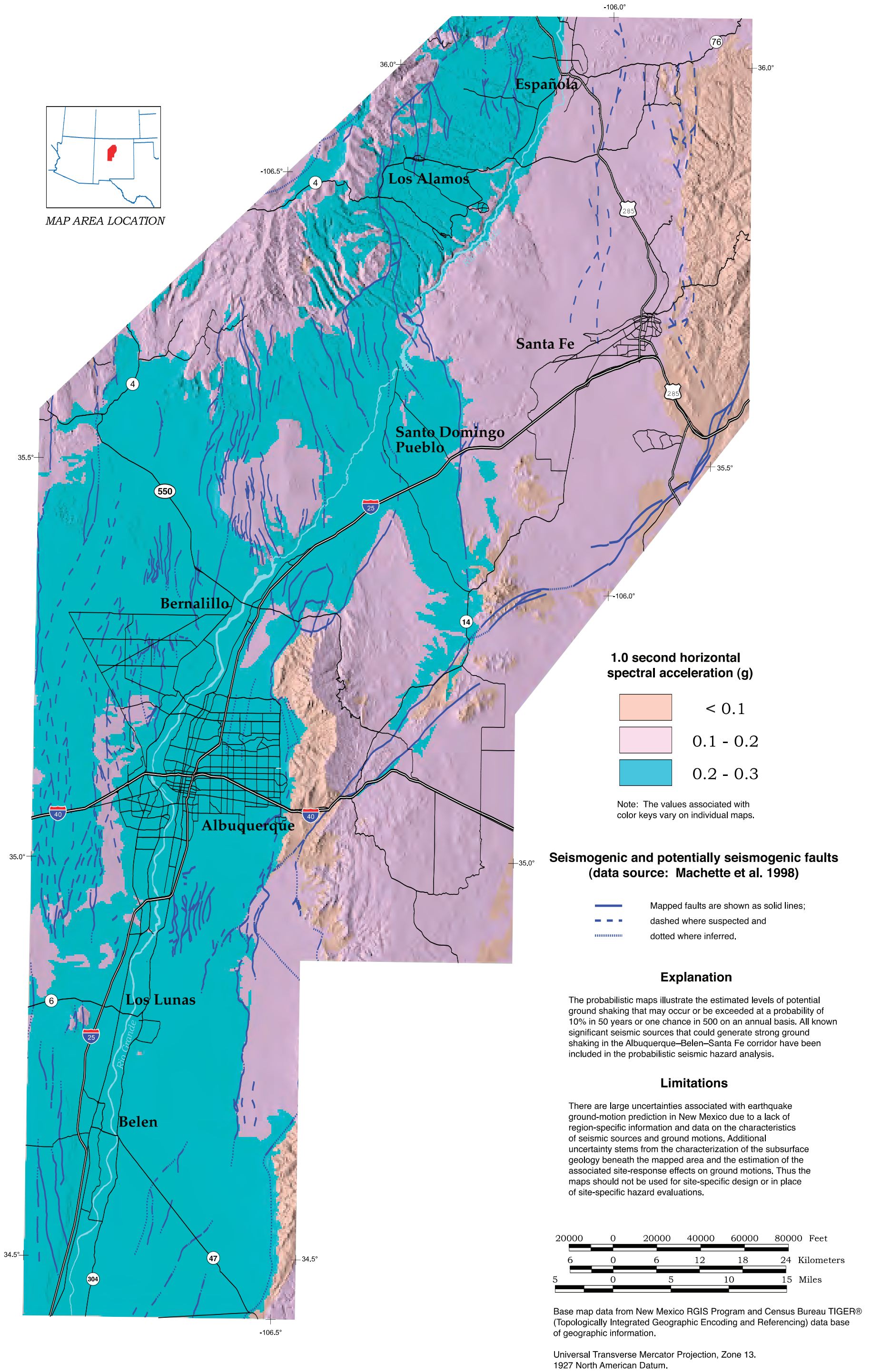

FIGURE 12—Probabilistic earthquake ground-shaking map for the Albuquerque–Belen–Santa Fe corridor, 10% probability of exceedance in 50 yrs, 1.0 sec horizontal spectral acceleration at the ground surface.

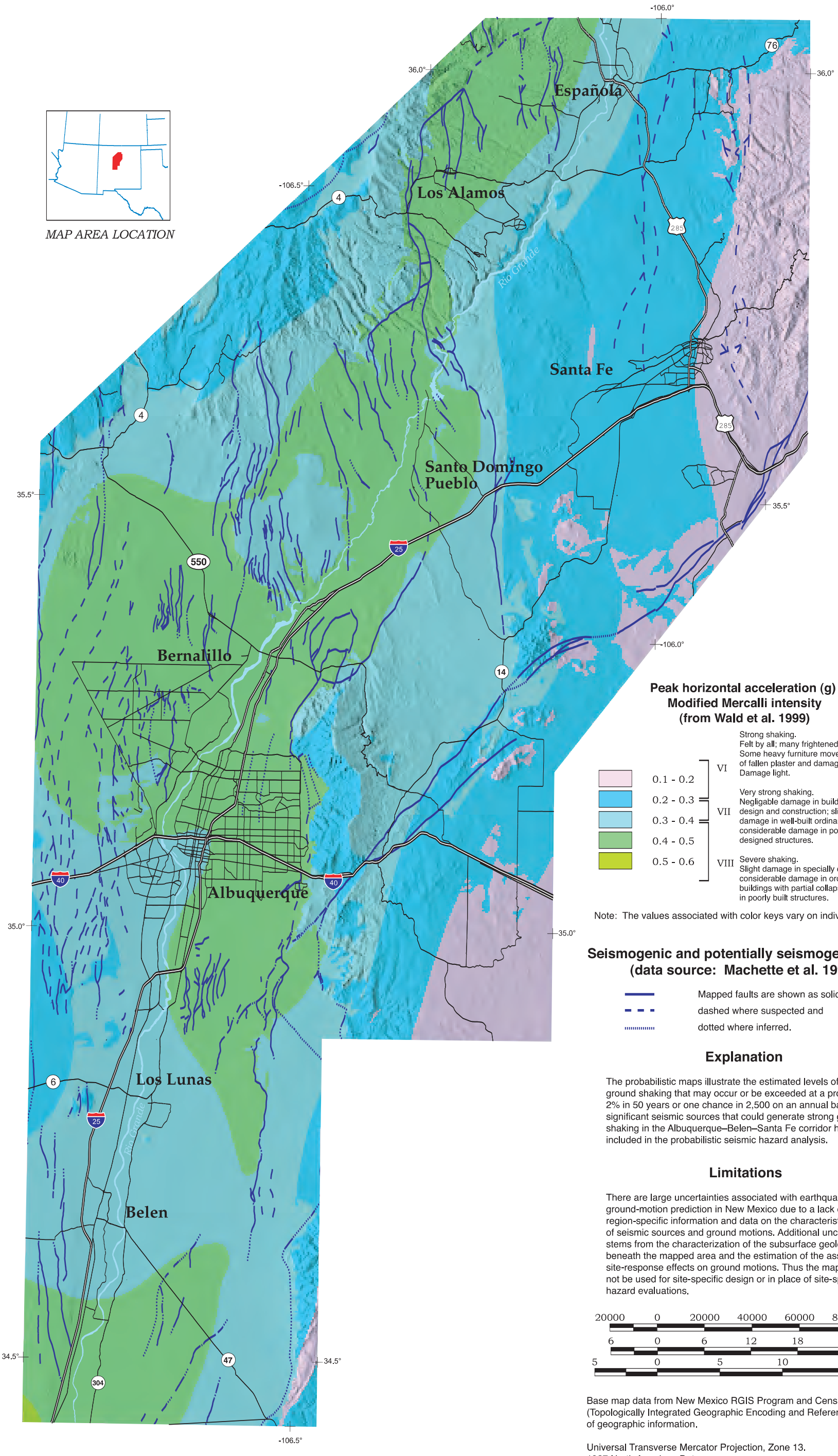

FIGURE 13—Probabilistic earthquake ground-shaking map for the Albuquerque–Belen–Santa Fe corridor, 2% probability of exceedance in 50 yrs, peak horizontal acceleration at the ground surface.

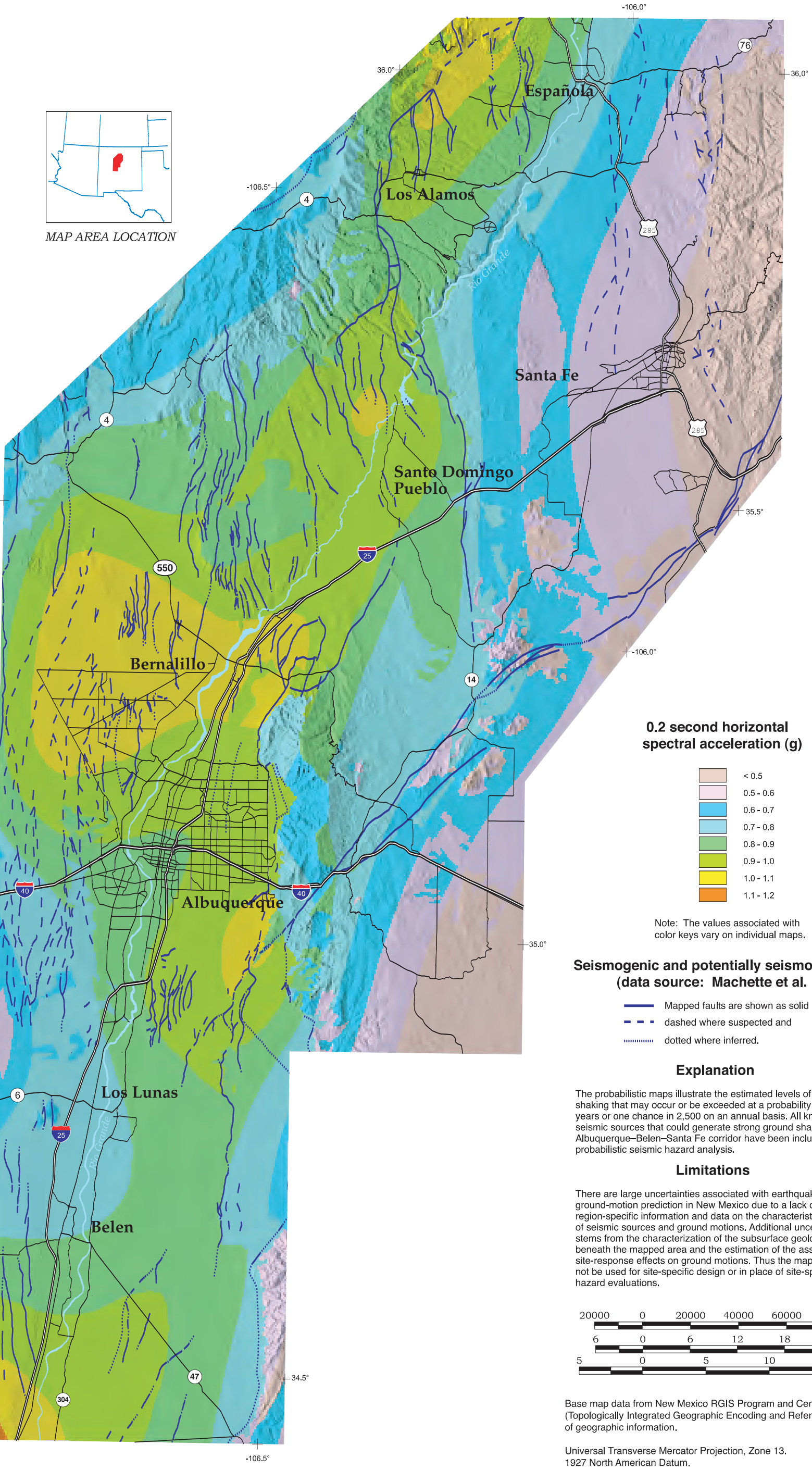

0.2 second horizontal spectral acceleration (g)

- < 0.5
- 0.5 - 0.6
- 0.6 - 0.7
- 0.7 - 0.8
- 0.8 - 0.9
- 0.9 - 1.0
- 1.0 - 1.1
- 1.1 - 1.2

Note: The values associated with color keys vary on individual maps.

Seismogenic and potentially seismogenic faults (data source: Machette et al. 1998)

Mapped faults are shown as solid lines;
dashed where suspected and
dotted where inferred.

Explanation

The probabilistic maps illustrate the estimated levels of potential ground shaking that may occur or be exceeded at a probability of 2% in 50 years or one chance in 2,500 on an annual basis. All known significant seismic sources that could generate strong ground shaking in the Albuquerque–Belen–Santa Fe corridor have been included in the probabilistic seismic hazard analysis.

Limitations

There are large uncertainties associated with earthquake ground-motion prediction in New Mexico due to a lack of region-specific information and data on the characteristics of seismic sources and ground motions. Additional uncertainty stems from the characterization of the subsurface geology beneath the mapped area and the estimation of the associated site-response effects on ground motions. Thus the maps should not be used for site-specific design or in place of site-specific hazard evaluations.

20000 0 20000 40000 60000 80000 Feet
6 0 6 12 18 24 Kilometers
5 0 5 10 15 Miles

Base map data from New Mexico RGIS Program and Census Bureau TIGER® (Topologically Integrated Geographic Encoding and Referencing) data base of geographic information.

Universal Transverse Mercator Projection, Zone 13.
1927 North American Datum.

FIGURE 14—Probabilistic earthquake ground-shaking map for the Albuquerque–Belen–Santa Fe corridor, 2% probability of exceedance in 50 yrs, 0.2 sec horizontal spectral acceleration at the ground surface.

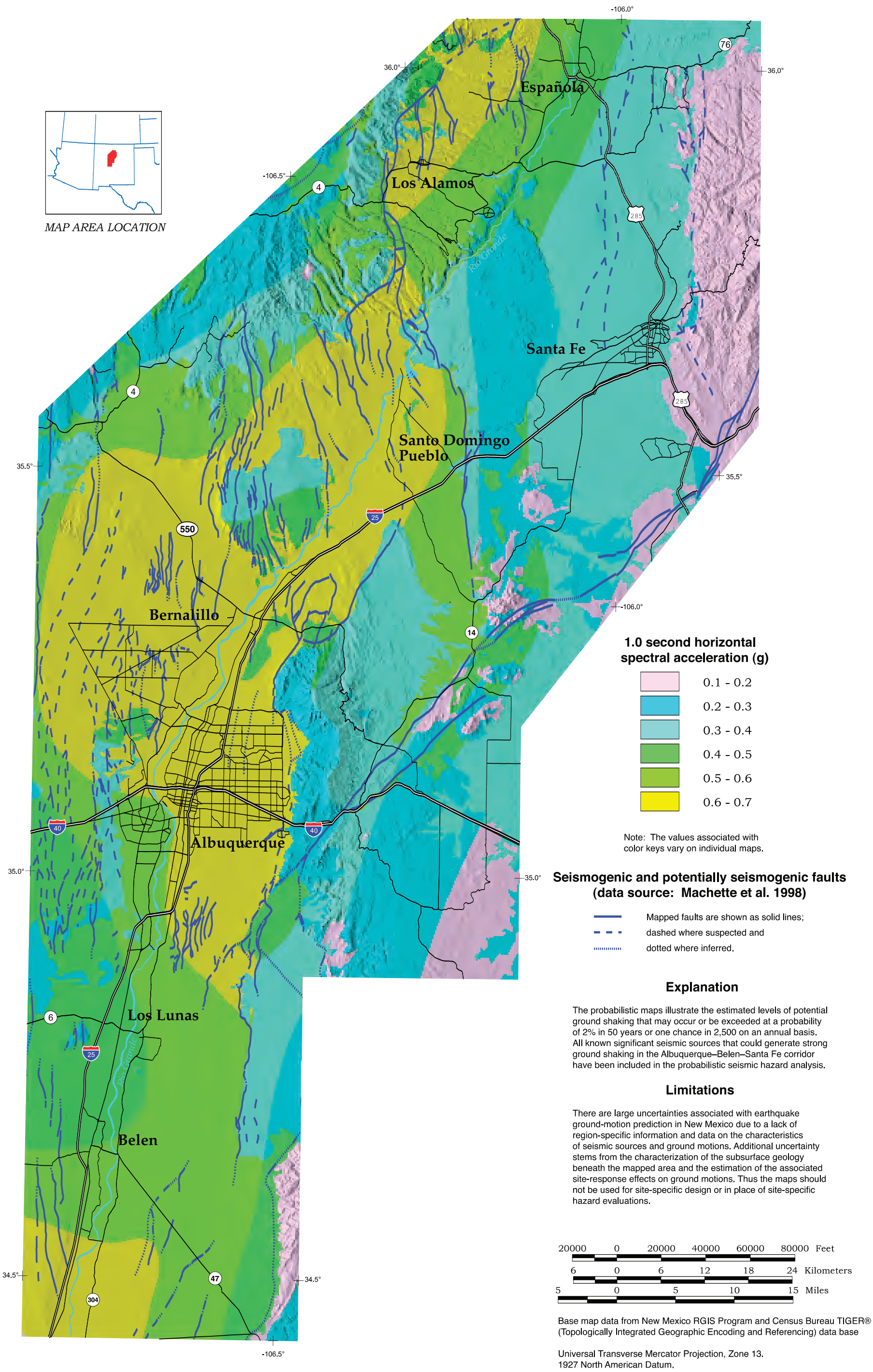

FIGURE 15—Probabilistic earthquake ground-shaking map for the Albuquerque–Belen–Santa Fe corridor, 2% probability of exceedance in 50 yrs, 1.0 sec horizontal spectral acceleration at the ground surface.